PHYSICAL REVIEW FLUIDS **10**, 124801 (2025)

Editors' Suggestion

Resonant triad interactions of two-layer gravity waves in cylindrical basins

Matthew Durey [*]
School of Mathematics and Statistics, University of Glasgow, University Place, Glasgow G12 8QQ, United Kingdom

Paul A. Milewski
Department of Mathematics, Pennsylvania State University, University Park, Pennsylvania 16802, USA

(Received 10 July 2025; accepted 24 October 2025; published 3 December 2025)

We present the results of a theoretical investigation into the existence and evolution of resonant triads of two-layer gravity waves confined to a cylinder of finite height. We consider a stable stratification, for which the lighter fluid lies above the heavier fluid, with the two fluids being separated by an interface and bounded above and below by rigid horizontal lids. We demonstrate that the lateral confinement can excite resonant three-wave interactions, resulting in pronounced interfacial sloshing and highly efficient energy exchange. Such interactions are absent in unbounded domains or rectangular cylinders and consist of a single vertical mode and a single interface. For a cylinder of arbitrary cross section, we prove necessary and sufficient conditions for three spatially correlated wave modes to resonate, with the existence of triads depending critically on the depth and density of each fluid. Upon deriving amplitude equations governing the long-time evolution of a resonant triad, we show that the triad evolution is generally periodic and determine conditions for which energy exchange is most propitious. We also identify a criticality condition exclusive to multilayer flows that describes the decoupling of the triad interaction. Finally, we discuss the implications of our findings on the formation of resonant internal wave interactions in geophysical basins.

DOI: 10.1103/m657-9blf

I. INTRODUCTION

Vertical mixing of salt and thermal energy within oceans plays a key role in regulating the world's climate and determining the flow of oceanic currents [1]. Variations in salinity and temperature typically lead to density stratification, for which the density of sea water may be parametrized by the fluid depth (see Sec. 1 in Ref. [2]). The resultant oceanic flows depend on the form of the vertical density profile: continuous stratification leads to pronounced vertical propagation [3], whereas sharp changes in density at a pycnocline support horizontally propagating internal waves [4], which play an important role in transporting energy over long distances compared to the vertical scales. In oceanography, the density stratification across pycnoclines is often modelled by a series of constant-density layers, each separated by a deformable interface (see Sec. 8 in

[*]Contact author: matthew.durey@glasgow.ac.uk

Ref. [5]). This class of multilayer model provides both analytical and computational benefits and has been used to rationalize internal solitary waves [6,7] and the interaction between free-surface and internal waves [4,8]. Owing to their relative simplicity, multilayer models serve as the basis for our investigation.

Stratified flows and oceanic mixing are enhanced by resonant coupling and concomitant energy exchange between the system's wave modes. This resonant coupling is particularly potent for the collective interaction of three wave modes, known as a resonant triad, for which intermode energy exchange is an order of magnitude faster than for the four-wave interactions prevalent at the ocean surface [9–11]. When the stratification is continuous, resonant triads are ubiquitous and consist of interacting horizontal and vertical wave modes [3,12–15]. For two-layer flows, resonant triads form between either two free surface wave modes and one internal mode [4,16–18] or between one free surface wave mode and two internal modes [8,19]. Akin to their single-layer counterparts [9,20], however, resonant triads in the ocean cannot consist of three wave modes all at the same interface, either at the free surface or at a deep pycnocline.

When water is confined to a lake or a harbor, the dominant wave modes are large-scale standing waves that span the basin, leading to dynamics distinct from laterally propagating ocean flows. For example, when strong winds blow across the surface of a large lake, the resultant subsurface flow can drive sustained internal oscillations of the lake's pycnocline, a phenomenon known as an internal seiche [21]. As lateral confinement is known to excite resonant triads of standing waves at an air-liquid interface [22,23], might it be possible for resonant triads to form solely at a pycnocline in a confined basin, without the need for coupling between interfaces or vertical modes? Such triads would present a new mechanism for resonantly coupling internal wave modes in geophysical basins and might explain the concurrent longitudinal and transverse internal seiching observed in lakes and harbors [21]. To test this possibility, we investigate herein the existence and evolution of resonant triads for the model problem of two-layer gravity waves confined laterally to a cylinder of arbitrary cross section. The flow is also confined vertically by a rigid base and lid, as is applicable when the amplitude of the internal wave greatly exceeds the free-surface displacement and variations in the bathymetry. As resonant triads are impossible for such flows in the absence of lateral confinement (see Appendix A), their excitation would be driven solely by the confining walls.

The formation of resonant triads in confined basins involves a subtle interplay between the system's wave modes and the basin geometry. For gravity waves at an air-liquid interface in a cylindrical basin, not all combinations of wave modes may form a resonant triad, and those that can form a triad do so only when the liquid depth is tuned judiciously [23–26]. Furthermore, the shape of the cylinder cross section plays a significant role: resonant triads are abundant for circular and annular cross sections [23], for example, yet are impossible for rectangular cylinders (for which the wave modes are a subset of plane gravity waves, which are known not to form triads [9,20]). Finally, the timescale of the triad evolution can vary significantly between different triads, with the slowest energy exchange emerging for shallow basins or for short-wave–long-wave interactions [23]. We anticipate similar constraints to emerge for resonant triads in two-layer flows, with a potentially complex dependence of the existence criteria and evolution timescale on the system's control parameters, specifically the density ratio and relative liquid depths.

We present herein a comprehensive characterization of resonant triads for two-layer gravity waves in a cylindrical basin of arbitrary cross section with a rigid lid and base. We outline the governing equations for confined two-layer gravity waves in Sec. II, which we simplify for the case of small-amplitude waves in Sec. III. Doing so determines the system's dispersion relation, which we analyze in Sec. IV to prove precise conditions for the existence of resonant triads. Particular attention is paid to the dependence of the triad existence criteria on the density ratio and relative fluid depth. Using the method of multiple scales, we characterize the long-time triad evolution in Sec. V and highlight some special cases of interest. We also identify a criticality condition that

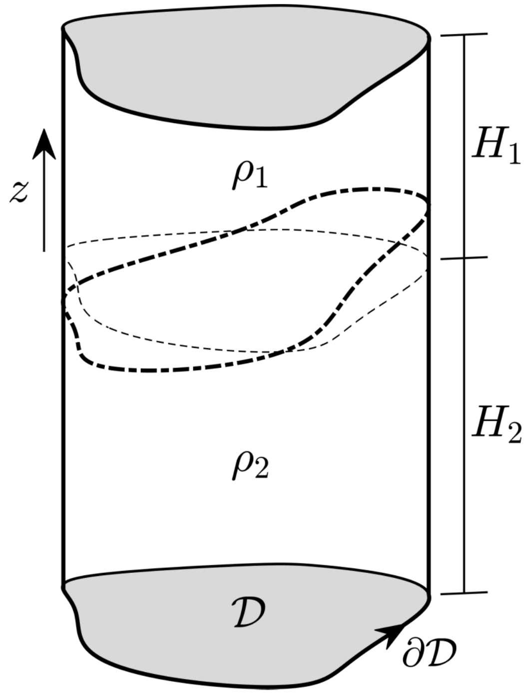

FIG. 1. Schematic diagram of the cylindrical basin (with cross section $\mathcal{D}$ and boundary $\partial\mathcal{D}$) partially filled with fluids of densities ρ_1 and ρ_2. The lighter fluid lies above the heavier fluid ($\rho_1 < \rho_2$), with the two fluids separated by an interface (dash-dotted curve) and bounded above and below by rigid horizontal lids (gray). When the system is at rest, the undisturbed free surface (dashed curve) lies at $z = 0$, a distance H_1 below the upper lid and H_2 above the lower lid.

describes the decoupling of a triad for certain parameter combinations, a phenomenon impossible for one-layer flows. Finally, we discuss our results in the context of geophysical flows in Sec. VI.

II. TWO-LAYER FLOWS IN A CYLINDER

We consider the evolution of two immiscible, incompressible, inviscid and irrotational fluids confined to a finite-depth vertical cylinder with cross section $\mathcal{D}$, configured in a stable stratification (see Fig. 1). We denote the interface between the two fluids by $z = \eta(\boldsymbol{x}, t)$, where $\boldsymbol{x}$ is the horizontal spatial coordinate, z is the vertical spatial coordinate, and t denotes time. The upper fluid (denoted with subscript 1) is confined above by a rigid horizontal lid at $z = H_1$, while the lower fluid (denoted with subscript 2) is confined below by a second lid at $z = -H_2$, with $\eta = 0$ when both fluids are at rest. We denote the density of each fluid by ρ_1 and ρ_2, where $\rho_1 < \rho_2$ for the stable stratification considered here.

A. Governing equations

The evolution of the two fluids is governed by the following system of equations (see Sec. 2 in Ref. [2]). For all $\boldsymbol{x} \in \mathcal{D}$, the velocity potentials, $\phi_l(\boldsymbol{x}, z, t)$, for the upper ($l = 1$) and lower ($l = 2$) layers satisfy the continuity equation

$$\Delta\phi_1 + \partial_{zz}\phi_1 = 0 \quad \text{for} \quad \eta(\boldsymbol{x}, t) < z < H_1, \tag{1a}$$

$$\Delta\phi_2 + \partial_{zz}\phi_2 = 0 \quad \text{for} \quad -H_2 < z < \eta(\boldsymbol{x}, t). \tag{1b}$$

On the interface, the fluids satisfy the kinematic boundary conditions

$$\frac{\partial \eta}{\partial t} + \boldsymbol{\nabla}\phi_1 \cdot \boldsymbol{\nabla}\eta = \partial_z \phi_1 \quad \text{on} \quad z = \eta(\boldsymbol{x}, t), \tag{1c}$$

$$\frac{\partial \eta}{\partial t} + \boldsymbol{\nabla}\phi_2 \cdot \boldsymbol{\nabla}\eta = \partial_z \phi_2 \quad \text{on} \quad z = \eta(\boldsymbol{x}, t), \tag{1d}$$

and the continuity of pressure across the interface gives rise to the dynamic boundary condition

$$\rho_1\left(\frac{\partial \phi_1}{\partial t} + \frac{1}{2}|\nabla\phi_1|^2 + \frac{1}{2}(\partial_z\phi_1)^2 + g\eta\right)$$
$$= \rho_2\left(\frac{\partial \phi_2}{\partial t} + \frac{1}{2}|\nabla\phi_2|^2 + \frac{1}{2}(\partial_z\phi_2)^2 + g\eta\right) \quad \text{on} \quad z = \eta(\boldsymbol{x}, t). \tag{1e}$$

In the above equations, $\boldsymbol{\nabla}$ and Δ denote the horizontal gradient and Laplacian operators, respectively, and g denotes the acceleration due to gravity. The fluid also satisfies no-flux conditions on the vertical walls of the cylinder, namely

$$\boldsymbol{\nabla}\phi_1 \cdot \boldsymbol{n} = 0 \quad \text{on} \quad \boldsymbol{x} \in \partial\mathcal{D} \quad \text{and} \quad \eta(\boldsymbol{x}, t) < z < H_1, \tag{1f}$$

$$\boldsymbol{\nabla}\phi_2 \cdot \boldsymbol{n} = 0 \quad \text{on} \quad \boldsymbol{x} \in \partial\mathcal{D} \quad \text{and} \quad -H_2 < z < \eta(\boldsymbol{x}, t), \tag{1g}$$

where $\boldsymbol{n}$ denotes the outward-pointing unit vector to the cylinder boundary, $\partial\mathcal{D}$. Finally, the no-flux condition on the horizontal plates at the base and lid of the cylindrical container correspond to

$$\partial_z\phi_1 = 0 \quad \text{on} \quad \boldsymbol{x} \in \mathcal{D} \quad \text{and} \quad z = H_1, \tag{1h}$$

$$\partial_z\phi_2 = 0 \quad \text{on} \quad \boldsymbol{x} \in \mathcal{D} \quad \text{and} \quad z = -H_2. \tag{1i}$$

As is implicit for the water-wave problem, we assume that the interface moves freely along vertical walls, remaining perpendicular to the wall for all time, i.e., $\boldsymbol{\nabla}\eta \cdot \boldsymbol{n} = 0$ on $\boldsymbol{x} \in \partial\mathcal{D}$ [27]. Finally, we note that the two-layer system (1) conserves mass, with $\iint_{\mathcal{D}} \eta \,\mathrm{d}A = 0$ for all time, where $\mathrm{d}A$ denotes the area element associated with integration across the cylinder cross section.

B. Weakly stratified flows

Our study encompasses the full range of relative densities, $\rho = \rho_1/\rho_2 < 1$, from strongly stratified flows, $\rho \ll 1$, such as at a liquid-air interface, to weakly stratified flows, $0 < 1 - \rho \ll 1$. The latter limit provides an informative point of comparison to the Boussinesq approximation, for which density differences are neglected in the dynamic boundary condition for all inertial terms and kept only in the buoyancy force [28]. This approximation, which is valid when $0 < 1 - \rho \ll 1$, thus reduces the dynamic boundary condition (1e) to the form

$$\frac{\partial \phi_1}{\partial t} + \frac{1}{2}|\nabla\phi_1|^2 + \frac{1}{2}(\partial_z\phi_1)^2 - \left(\frac{\partial \phi_2}{\partial t} + \frac{1}{2}|\nabla\phi_2|^2 + \frac{1}{2}(\partial_z\phi_2)^2\right)$$
$$+ (1-\rho)g\eta = 0 \quad \text{on} \quad z = \eta(\boldsymbol{x}, t). \tag{2}$$

We note from (2) two observations that will feature throughout our analysis of resonant triads. First, we observe that gravity waves evolve over the timescale $\sqrt{a/(1-\rho)g}$ for weakly stratified flows, where a is the typical length scale of the cylinder cross section. Consequently, if resonant triads were to exist in this limit for a particular cylinder geometry, then the evolution timescale would diverge when the stratification is weakened progressively. Second, we observe that the Boussinesq system [consisting of Eqs. (1a)–(1d), (1f)–(1i), and (2)] is invariant under the mapping

$$z \mapsto -z, \quad \eta \mapsto -\eta, \quad H_1 \longleftrightarrow H_2 \quad \text{and} \quad 1-\rho \longleftrightarrow -(1-\rho).$$

For any solution identified in the original system, there thus exists a second solution found by reflecting about $z = 0$ and reassigning the layer densities and depths. This invariance may be made more explicit by denoting the densities in the original system as $\rho_2 = \rho_*$ and $\rho_1 = \rho_* - \Delta\rho$: The Boussinesq approximation then determines that a new system with lower depth H_1 and upper depth H_2, and respective densities $\rho_* + \Delta\rho$ and ρ_*, exhibits exactly the same dynamics as the original system.

C. Strongly stratified flows

When the density of the upper layer is small relative to that of the lower layer, $\rho \ll 1$, such as at an air-liquid interface, the dynamic boundary condition (1e) may be approximated by

$$\frac{\partial \phi_2}{\partial t} + \frac{1}{2}|\nabla\phi_2|^2 + \frac{1}{2}(\partial_z\phi_2)^2 + g\eta = 0 \quad \text{on} \quad z = \eta(\boldsymbol{x}, t). \tag{3}$$

Consequently, the velocity potential for the upper layer, ϕ_1, partially decouples from the system: η and ϕ_2 may first be solved as a one-layer system, the solution to which determines ϕ_1. We thus anticipate that the two-layer system will evolve similarly to the one-layer system for strongly stratified flows, for which resonant triads were found to be abundant for nonrectangular cylinders [23].

III. SMALL-AMPLITUDE WAVES

We proceed by expanding the governing equations (1) in the limit for which the characteristic wave slope, ϵ, is small, i.e., $0 < \epsilon \ll 1$. By taking the typical length scale, a, of the cylinder cross section as the unit of length, and $\sqrt{a/g}$ as the unit of time, we nondimensionalize the governing equations (1) and perform Taylor expansions in ϵ of the boundary conditions (1c)–(1e) about $z = 0$. Specifically, we define the dimensional quantities in terms of their dimensionless counterparts (denoted by overhead bars) according to $(\boldsymbol{x}, z) = a(\bar{\boldsymbol{x}}, \bar{z})$, $t = \sqrt{a/g}\,\bar{t}$, $\phi_l = \epsilon a\sqrt{ag}\bar{\phi}_l$ (for $l = 1, 2$), and $\eta = \epsilon a\bar{\eta}$. The dynamics of the dimensionless fluid system is then characterized in terms of the density ratio, $\rho = \rho_1/\rho_2$, and the aspect ratio, $h_l = H_l/a$ (for $l = 1, 2$), of each fluid. Throughout the following analysis, we treat ρ and h_l as fixed parameters as $\epsilon \to 0$ [i.e., $\rho = O(1)$ and $h_l = O(1)$], with $0 < \rho < 1$ and $0 < h_l < \infty$.

Upon dropping overhead bars on dimensionless variables and denoting $u_l(\boldsymbol{x}, t) = \phi_l(\boldsymbol{x}, 0, t)$ for $l = 1, 2$, we expand the kinematic boundary conditions (1c) and (1d) to deduce that

$$\frac{\partial \eta}{\partial t} + \mathscr{L}_1 u_1 + \epsilon\nabla\cdot(\eta\nabla u_1) = O(\epsilon^2) \quad \text{for} \quad \boldsymbol{x} \in \mathcal{D}, \tag{4a}$$

$$\frac{\partial \eta}{\partial t} - \mathscr{L}_2 u_2 + \epsilon\nabla\cdot(\eta\nabla u_2) = O(\epsilon^2) \quad \text{for} \quad \boldsymbol{x} \in \mathcal{D}, \tag{4b}$$

where $\mathscr{L}_1$ and $\mathscr{L}_2$ are the Dirichlet-to-Neumann operators on $z = 0$ for Laplace's equation on the linearized domains $\boldsymbol{x} \in \mathcal{D}$ with $0 < z < h_1$ or $-h_2 < z < 0$, respectively. Specifically, $\mathscr{L}_1 u_1 = -\partial_z\phi_1|_{z=0}$ for ϕ_1 satisfying Laplace's equation (1a) over the interval $0 < z < h_1$ with no-flux boundary conditions on the lid, i.e., $\partial_z\phi_1 = 0$ on $z = h_1$ [see (1h)], and side walls, i.e., $\boldsymbol{n}\cdot\nabla\phi_1 = 0$ for $\boldsymbol{x} \in \partial\mathcal{D}$ [see (1f)]. Likewise, $\mathscr{L}_2 u_2 = +\partial_z\phi_2|_{z=0}$ for ϕ_2 satisfying Laplace's equation (1b) over the interval $-h_2 < z < 0$ with no-flux boundary conditions on the base, i.e., $\partial_z\phi_2 = 0$ on $z = -h_2$ [see (1i)], and side walls, i.e., $\boldsymbol{n}\cdot\nabla\phi_2 = 0$ for $\boldsymbol{x} \in \partial\mathcal{D}$ [see (1g)]. The dynamic boundary condition (1e) is likewise expanded as

$$\begin{aligned}&\rho\left(\frac{\partial u_1}{\partial t} + \eta + \epsilon\left[-\eta\frac{\partial}{\partial t}(\mathscr{L}_1 u_1) + \frac{1}{2}|\nabla u_1|^2 + \frac{1}{2}(\mathscr{L}_1 u_1)^2\right]\right)\\ &\quad = \frac{\partial u_2}{\partial t} + \eta + \epsilon\left[\eta\frac{\partial}{\partial t}(\mathscr{L}_2 u_2) + \frac{1}{2}|\nabla u_2|^2 + \frac{1}{2}(\mathscr{L}_2 u_2)^2\right] + O(\epsilon^2) \quad \text{for} \quad \boldsymbol{x} \in \mathcal{D}.\end{aligned} \tag{4c}$$

A. Eigenmode decomposition

A convenient representation of the Dirichlet-to-Neumann operators, $\mathscr{L}_1$ and $\mathscr{L}_2$, is in terms of an orthonormal set of eigenfunctions of the Laplacian operator on the domain prescribed by the cylinder cross section, $\mathcal{D}$, equipped with no-flux boundary conditions on the boundary, $\partial\mathcal{D}$ [25]. Specifically, we consider the complete set of real-valued eigenfunctions, $\Phi_n(\boldsymbol{x})$ (for $n = 0, 1, 2, \ldots$), satisfying

$$-\Delta\Phi_n = k_n^2\Phi_n \quad \text{for} \quad \boldsymbol{x} \in \mathcal{D},$$

with $\boldsymbol{n} \cdot \nabla\Phi_n = 0$ for $\boldsymbol{x} \in \partial\mathcal{D}$. Notably, the eigenfunctions are orthogonal with respect to the inner product

$$\langle f, g\rangle = \frac{1}{S}\iint_{\mathcal{D}} f g \,\mathrm{d}A,$$

namely $\langle\Phi_m, \Phi_n\rangle = \delta_{mn}$, where S denotes the area of the cylinder cross section, $\mathcal{D}$. Finally, we order the eigenvalues, k_n^2, so that $0 = k_0 < k_1 \leqslant k_2 \leqslant \ldots$. Upon representing $u_l(\boldsymbol{x}, t) = \sum_{n=0}^{\infty}\hat{u}_{l,n}(t)\Phi_n(\boldsymbol{x})$ for $l = 1, 2$, each Dirichlet-to-Neumann operator may be written as $\mathscr{L}_l u_l = \sum_{n=0}^{\infty}\hat{\mathscr{L}}_{l,n}\hat{u}_{l,n}\Phi_n$, where

$$\hat{\mathscr{L}}_{l,n} = k_n\tanh(k_n h_l)$$

is the spectral multiplier of $\mathscr{L}_l$.

B. Dispersion relation

Although the dispersion relation for two-layer flow is well known (see Sec. 231 in Ref. [29]), it is informative to briefly recall the derivation here so as to motivate the methodologies utilized in the weakly nonlinear analysis presented in Sec. V. In the limit $\epsilon \to 0$, the expanded system (4) forms a set of three linear differential equations whose projection onto the orthogonal eigenfunctions, Φ_n, determines that $\hat{\eta}_n = \langle\Phi_n, \eta\rangle$ and $\hat{u}_{j,n} = \langle\Phi_n, u_j\rangle$ evolve according to

$$\frac{\mathrm{d}\hat{\eta}_n}{\mathrm{d}t} + \hat{\mathscr{L}}_{1,n}\hat{u}_{1,n} = 0, \tag{5a}$$

$$\frac{\mathrm{d}\hat{\eta}_n}{\mathrm{d}t} - \hat{\mathscr{L}}_{2,n}\hat{u}_{2,n} = 0, \tag{5b}$$

$$\frac{\mathrm{d}}{\mathrm{d}t}(\hat{u}_{2,n} - \rho\hat{u}_{1,n}) + (1-\rho)\hat{\eta}_n = 0. \tag{5c}$$

We note that additive invariance of each velocity potential implies that we may set $\hat{u}_{l,0} = 0$ without loss of generality (for $l = 1, 2$), and that conservation of mass corresponds to setting $\hat{\eta}_0 = 0$. Furthermore, one may combine (5a) and (5b) to express $\hat{u}_{1,n}$ in terms of $\hat{u}_{2,n}$ for all $n > 0$, thereby indicating that the system (5) is degenerate. We thus reduce (5) to two linearly independent differential equations describing the evolution of the variables $\hat{\xi}_n(t) = (1-\rho)\hat{\eta}_n(t)$ and $\hat{\varphi}_n(t) = \hat{u}_{2,n}(t) - \rho\hat{u}_{1,n}(t)$. Specifically, we combine the kinematic boundary conditions (5a) and (5b) to deduce that

$$\frac{\mathrm{d}\hat{\xi}_n}{\mathrm{d}t} - \frac{(1-\rho)\hat{\mathscr{L}}_{1,n}\hat{\mathscr{L}}_{2,n}}{\hat{\mathscr{L}}_{1,n} + \rho\hat{\mathscr{L}}_{2,n}}\hat{\varphi}_n = 0 \tag{6a}$$

and the dynamic boundary condition (5c) is recast as

$$\frac{\mathrm{d}\hat{\varphi}_n}{\mathrm{d}t} + \hat{\xi}_n = 0. \tag{6b}$$

Solutions to the linear system (6) are of the form $e^{\pm i\omega_n t}$, where the angular frequency, ω_n, satisfies

$$\omega_n^2 = \frac{(1-\rho)\hat{\mathscr{L}}_{1,n}\hat{\mathscr{L}}_{2,n}}{\hat{\mathscr{L}}_{1,n} + \rho\hat{\mathscr{L}}_{2,n}}, \quad \text{or} \quad \omega_n^2 = \frac{(1-\rho)k_n}{\rho\coth(k_n h_1) + \coth(k_n h_2)}. \tag{7}$$

As $\omega_0 = 0$ and $\hat{u}_{l,0} = \hat{\eta}_0 = 0$, we exclude the wave number $k_0 = 0$ [corresponding to the eigenfunction $\Phi_0(\boldsymbol{x}) = 1$] from further consideration: We thus consider only positive wave numbers, $k_n > 0$, henceforth.

IV. EXISTENCE OF RESONANT TRIADS

To determine conditions for which resonant triads form, we consider three linear wave modes, enumerated n_1, n_2, and n_3, with spatial profiles $\Psi_j(\boldsymbol{x}) = \Phi_{n_j}(\boldsymbol{x})$, wave numbers $K_j = k_{n_j} > 0$, and angular frequencies $\Omega_j = \omega_{n_j}$ for $j = 1, 2, 3$. In this notation, the dispersion relation (7) becomes

$$\Omega_j^2 = \frac{(1-\rho)K_j}{\rho\coth(K_j h_1) + \coth(K_j h_2)}, \tag{8}$$

where we define $\Omega_j > 0$ without loss of generality. For two-layer flow confined to a cylinder, three wave modes [upon suitable relabelling of the indices $(1, 2, 3)$] form a resonant triad when their angular frequencies satisfy the condition (see Sec. 5 in Ref. [30])

$$\Omega_1 + \Omega_2 = \Omega_3 \tag{9a}$$

and their spatial profiles, $\Psi_j(\boldsymbol{x})$, satisfy [23,25]

$$\iint_{\mathcal{D}} \Psi_1\Psi_2\Psi_3 \, \mathrm{d}A \neq 0. \tag{9b}$$

The first condition (9a) ensures that the product of any two of the wave modes oscillates at the frequency of the third wave mode, which can only be satisfied when $K_1 + K_2 < K_3$ for fluids of finite and positive depth (see Sec. IV A). The second condition (9b) ensures that products of two wave modes are nonorthogonal in space to the third wave mode, referred to as the correlation condition [23,25]. Notably, the correlation condition (9b) reduces to the condition $\boldsymbol{k}_1 + \boldsymbol{k}_2 = \boldsymbol{k}_3$ for plane waves with wave vectors $\boldsymbol{k}_j$ in a rectangular cylinder (or unbounded domain), which cannot be satisfied concurrently with the frequency condition (9a); see Appendix A. However, the distortion of the wave modes away from plane waves for nonrectangular cylinders allows for (9a) and (9b) to be satisfied simultaneously under certain conditions elucidated below. Finally, the slow timescale of the triad evolution is inversely proportional to the parameter Γ defined in Sec. V, necessitating that $\Gamma \neq 0$. This final condition is investigated in greater detail in Sec. V.

Despite the complex dependence of the angular frequency, Ω_j, on the fluid depths and the density ratio, preliminary insight may be gained into the existence of resonant triads through the consideration of different limits. For example, we anticipate that the triad existence criteria for two-layer flows will be similar to that of one-layer flows for strong stratification (see Sec. II C) or for very deep flows. The latter assertion may be justified by first noting that

$$\Omega_j^2 \sim K_j \frac{1-\rho}{1+\rho} \quad \text{for } K_j h_1 \gg 1 \text{ and } K_j h_2 \gg 1,$$

which reduces to the dispersion relation, $\Omega_j^2 \sim K_j$, for deep, single-layer flow upon a suitable rescaling of time. We also anticipate that resonant triads will not exist when the upper layer is very shallow, regardless of the depth of the lower layer. Specifically, the dispersion relation in this case reduces to

$$\Omega_j^2 \sim K_j^2 h_1 \frac{1-\rho}{\rho} \quad \text{for } K_j h_1 \ll 1,$$

which may be recast as the shallow-water, single-layer dispersion relation, $\Omega_j^2 \sim K_j^2$, upon rescaling time. As resonant triads do not exist in this limit for single-layer flows (i.e., for a finite and nonzero fluid depth, triads exist only when $K_1 + K_2 < K_3$ [23]), we expect the same to hold for two-layer flows with a shallow upper layer. A similar argument determines that resonant triads will not exist when the lower layer is very shallow, regardless of the depth of the upper layer.

The remainder of this section is focused on determining conditions for which the condition (9a) on the angular frequencies is satisfied, which we find depends critically on the parameters h_1, h_2, and ρ. We describe the dependence on the governing parameters in two different settings: (i) the influence of the upper layer (fixing ρ and h_1) on the necessary conditions on the lower depth, h_2, for a triad to form and (ii) the influence of the total cylinder height, denoted by $h = h_1 + h_2$, on the existence of resonant triads for a fixed density ratio, ρ. The former setting allows for a comparison to one-layer flows and the latter to the symmetries associated with Boussinesq flows.

A. The influence of the upper fluid on triad formation

In order to draw parallels to the existence of resonant triads for single-layer flows (corresponding to $\rho \to 0$), we fix the depth of the upper layer, $h_1 > 0$, and the density ratio, $0 < \rho < 1$ [23]. Necessary and sufficient conditions for the existence of a critical depth of the lower layer, h_2, at which the three wave modes resonate are summarized in Theorem 1.

Theorem 1. Consider three wave modes with wave numbers $K_1, K_2, K_3 > 0$. For given $h_1 > 0$ and $0 < \rho < 1$, there exists a positive and finite value of h_2 such that $\Omega_1 + \Omega_2 = \Omega_3$ [for $\Omega_j > 0$ defined in (8)] if and only if

$$K_1 + K_2 < K_3 \quad \text{and} \quad \sqrt{\frac{K_3}{1 + \rho \coth(K_3 h_1)}} < \sqrt{\frac{K_1}{1 + \rho \coth(K_1 h_1)}} + \sqrt{\frac{K_2}{1 + \rho \coth(K_2 h_1)}}. \tag{10}$$

When this pair of inequalities is satisfied, the critical value of h_2 is unique.

The proof of Theorem 1 follows a strategy similar to that of a single fluid layer [23], with details presented in Appendix B. Specifically, we first show that resonant triads are impossible for finite $h_2 > 0$ when $K_1 + K_2 \geqslant K_3$. Furthermore, the function $F(h_2) = (\Omega_1(h_2) + \Omega_2(h_2))/\Omega_3(h_2) - 1$, whose roots are the critical values of h_2 for given values of h_1 and ρ, is shown to be strictly monotonically increasing for $K_1 + K_2 < K_3$. The left-hand inequality in (10) corresponds to the condition $\lim_{h_2 \to 0} F(h_2) < 0$ and the right-hand inequality corresponds to the condition $\lim_{h_2 \to \infty} F(h_2) > 0$. The continuity of $F(h_2)$ thus guarantees that there exists at least one finite critical depth, satisfying $F(h_2) = 0$, when the inequalities (10) are satisfied. The strict monotonicity of $F(h_2)$ implies that any such critical depth must be unique, which completes the proof.

We present in Fig. 2 the triad existence region for different values of the density ratio, ρ, and the depth of the upper layer, h_1. For a triplet of wave numbers (K_1, K_2, K_3) contained within the existence region (10), there exists a unique critical depth at which a triad consisting of these wave modes forms, with the critical depth of the lower layer, h_2, increasing from right to left across the existence region. Outside of the existence region, resonant triads are impossible, regardless of the fluid depth. Increasing the density ratio towards unity shrinks the triad existence region, as does decreasing the depth of the upper layer. Specifically, the left-hand existence boundary approaches the line $K_3 = K_1 + K_2$ in the limit $h_1 \to 0$, and thus the triad existence region becomes infinitesimally thin. In contrast, the triad existence region remains of finite size as $\rho \to 1^-$, although the oscillation timescale of each wave mode becomes arbitrarily long [see (8)].

In accordance with our arguments above, the triad existence region approaches that of one-layer flows for a deep upper layer or for strong stratification. Specifically, the left-hand boundary approaches the curve $\sqrt{K_3} = \sqrt{K_1} + \sqrt{K_2}$ as $h_1 \to \infty$ or as $\rho \to 0$, which was found to be precisely the left-hand existence boundary for single-layer flow [23]. In fact, the triad existence region for two-layer flow is confined within the existence region for one-layer flow for all parameter values,

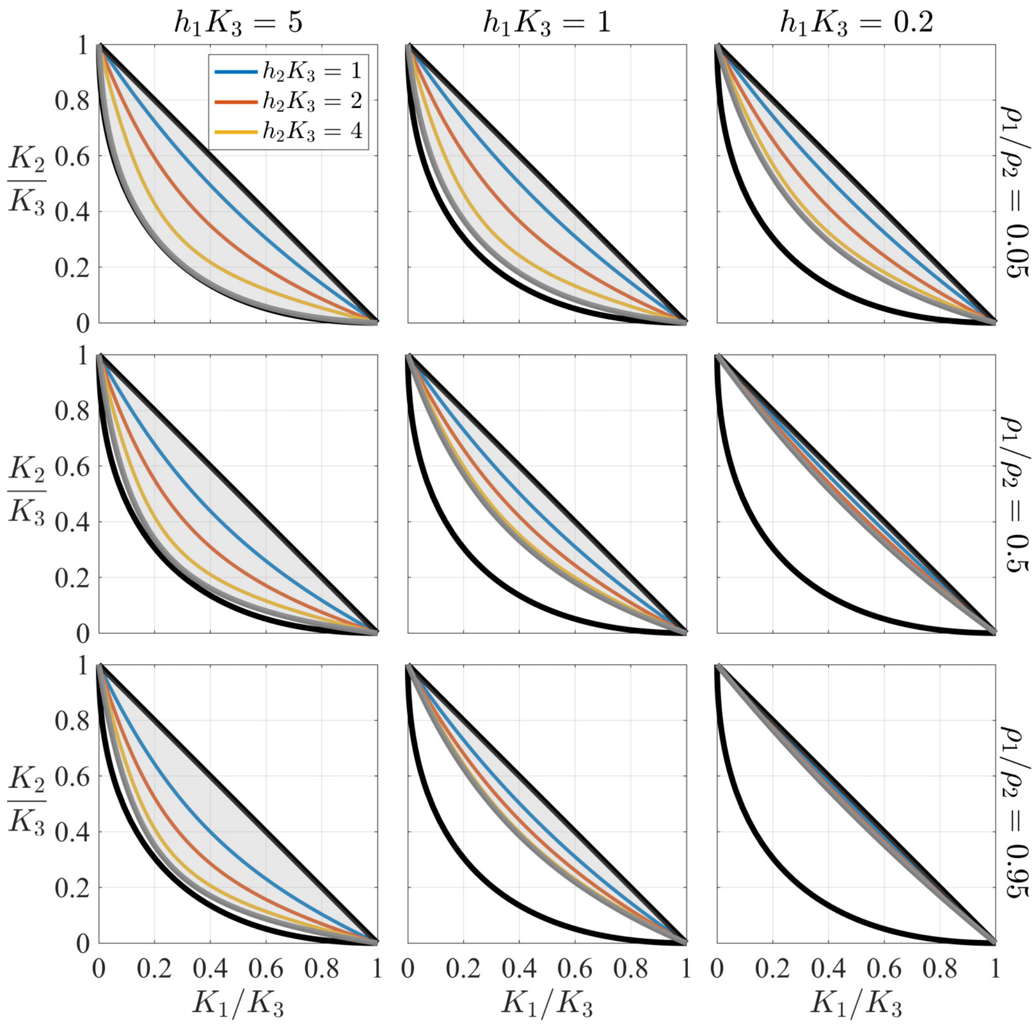

FIG. 2. Existence of resonant triads for stably stratified, two-layer flow in a cylinder. For fixed values of the density ratio, $\rho = \rho_1/\rho_2$, and the depth of the upper layer, h_1, a resonant triad exists when the wave numbers, K_j, lie within the gray shaded region defined by (10). Notably, the two-layer existence region is contained within the single-layer existence region (bounded by the black curves) for all parameter values (see Corollary 1). Contours of the corresponding critical depth of the lower layer, h_2, are superimposed on the existence region, with $h_2 \to 0$ on the right-hand boundary and $h_2 \to \infty$ on the left-hand boundary. The existence region vanishes as $h_1 \to 0$, but remains finite in size as $\rho \to 1$.

and thus a second layer suppresses the set of wave modes that can excite a resonant triad. We summarize this observation in the following corollary.

Corollary 1. For positive K_1, K_2, and K_3 satisfying the two-fluid triad existence criteria (10) for fixed $0 < \rho < 1$ and finite $h_1 > 0$, the single-fluid triad existence criteria (corresponding to $\rho \to 0$) are also satisfied, namely $K_1 + K_2 < K_3$ and $\sqrt{K_3} < \sqrt{K_1} + \sqrt{K_2}$.

Proof of Corollary 1. From (10), we see immediately that the inequality $K_1 + K_2 < K_3$ is satisfied. By rearranging the second inequality in (10), we deduce that

$$\sqrt{K_3} < \sqrt{K_1}\sqrt{\frac{1 + \rho\coth(K_3h_1)}{1 + \rho\coth(K_1h_1)}} + \sqrt{K_2}\sqrt{\frac{1 + \rho\coth(K_3h_1)}{1 + \rho\coth(K_2h_1)}}. \tag{11}$$

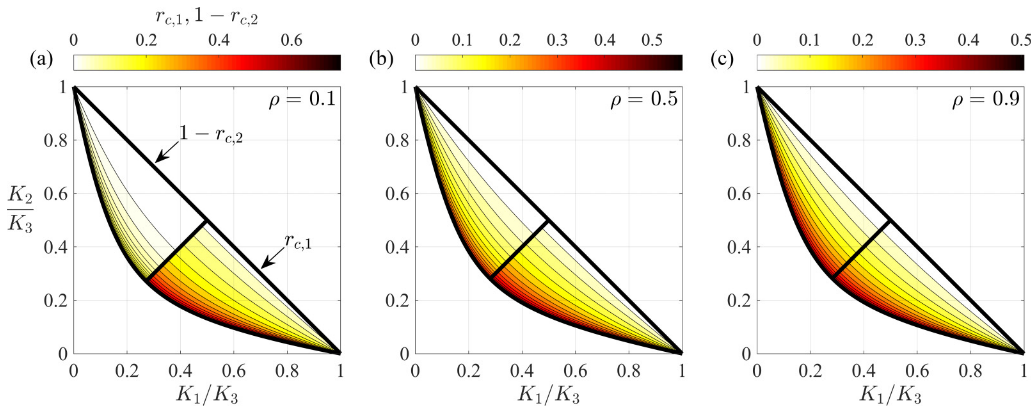

FIG. 3. The critical depths for resonant triads emerging within a cylinder of total height $K_3h = 10$. The density ratio assumes the values (a) $\rho = 0.1$, (b) $\rho = 0.5$, and (c) $\rho = 0.9$. The depth ratio, $0 < r < 1$, is defined so that the upper depth is $h_1 = (1 - r)h$ and the lower depth is $h_2 = rh$. Within the triad existence region, there are two critical depths, denoted $r_{c,1} < r_{c,2}$, both of which are symmetric about the line $K_1 = K_2$. For ease of visualization, we divide the existence region into two parts, with $r_{c,1} = h_2/h$ presented for $K_1 > K_2$ (lower right region), and $1 - r_{c,2} = h_1/h$ for $K_1 < K_2$ (upper left region). (a) For strongly stratified flows, $r_{c,2} \approx 1$ and thus the second critical depth approaches the upper lid. (c) For weakly stratified flows, the symmetry invariance of Boussinesq flows yields $r_{c,1} \approx 1 - r_{c,2}$ (see Sec. II B).

As $\coth(x)$ is a strictly decreasing function for $x > 0$, we use the inequality $K_j < K_3$ (for $j = 1, 2$) to note that $\coth(K_jh_1) > \coth(K_3h_1)$ and thus

$$\sqrt{\frac{1 + \rho\coth(K_3h_1)}{1 + \rho\coth(K_jh_1)}} < 1 \quad \text{for} \quad j = 1, 2.$$

By substituting these inequalities into the right-hand side of Eq. (11), we deduce that $\sqrt{K_3} < \sqrt{K_1} + \sqrt{K_2}$, as required. ■

B. The influence of the cylinder height on triad formation

The symmetry invariance of two-layer Boussinesq flows (see Sec. II B) implies that when the height of the cylinder, $h = h_1 + h_2$, is fixed, critical depths at which a triad may form emerge in symmetric pairs about the midline, specifically at depths h_c and $h - h_c$. To quantify the deviation from this relationship for more strongly stratified flows, we investigate the existence of resonant triads when $h = h_1 + h_2$ and the density ratio, ρ, are both fixed. To do so, we define the depth ratio, $0 < r < 1$, so that the height of the lower layer is $h_2/h = r$ and the height of the upper layer is $h_1/h = 1 - r$. The existence of critical depth ratios satisfying $\Omega_1 + \Omega_2 = \Omega_3$ is determined numerically using the algorithm outlined in Appendix C. For a given triplet of wave numbers (K_1, K_2, K_3) and density ratio, ρ, we find that there are either no values of r for which $\Omega_1 + \Omega_2 = \Omega_3$, or there are two solutions, enumerated so that $0 < r_{c,1} < r_{c,2} < 1$.

As presented in Fig. 3, the triad existence region in the $(K_1/K_3, K_2/K_3)$ plane resembles those delineated in Sec. IV A, bounded to the right by the line $K_1 + K_2 = K_3$ and to left by the curve along which $r_{c,1} = r_{c,2}$. As wave modes 1 and 2 are interchangeable, $r_{c,1}$ and $r_{c,2}$ are both symmetric about the line $K_1 = K_2$. To visualize both critical depths on the same plot, we thus present $r_{c,1}$ for $K_1 > K_2$ and $1 - r_{c,2}$ for $K_1 < K_2$, corresponding to the respective critical depths of the lower and upper layers. For Boussinesq flows, the symmetric pairing of critical depths about the midline ensures that $r_{c,1} \approx 1 - r_{c,2}$, as is evident in Fig. 3(c) for $\rho = 0.9$. As the density ratio is increased progressively, the difference between $r_{c,1}$ and $1 - r_{c,2}$ becomes more pronounced, with the critical depths thus deviating from a symmetric configuration. In particular, $r_{c,2} \to 1$ for strongly stratified flows [see Fig. 3(a)], corresponding to a critical depth close to the upper lid. In contrast, $r_{c,1}$ remains roughly constant as ρ varies, as does the triad existence region, which is bounded within $K_1 + K_2 < K_3 < (\sqrt{K_1} + \sqrt{K_2})^2$ (see Corollary 1). However, the triad existence region shrinks as the cylinder height is decreased, vanishing for shallow-layer flows.

V. EVOLUTION OF RESONANT TRIADS

For small-amplitude waves, for which $0 < \epsilon \ll 1$, weakly nonlinear effects play a significant role in the triad evolution over long timescales, specifically $t = O(\epsilon^{-1})$. We determine this long-time evolution by applying the method of multiple scales [31] to the two-layer wave equations (4), thus deriving a set of equations for the amplitude and phase of each wave mode in the triad. Notably, our weakly nonlinear analysis cannot describe the triad evolution for waves of larger amplitude (corresponding to moderate values of ϵ), for which more complex resonances are expected to be triggered. Nevertheless, our analysis gives insight into the relative efficiency of intratriad energy exchange for confined two-layer flows. In particular, we specify the dependence of the triad evolution timescale on the density ratio and fluid depths across the triad existence regions established in Sec. IV.

For algebraic convenience in the following analysis, we relax the condition that each angular frequency, Ω_j, must be positive, and instead consider the resonance condition $\Omega_1 + \Omega_2 + \Omega_3 = 0$ [32], for which each angular frequency can be positive or negative (but not equal to zero). The advantage of recasting the resonance condition in this form is that the cyclical symmetry of the angular frequencies is inherited by the resultant amplitude equations, thus giving structure to the accompanying coefficients [32]. Throughout the following analysis, we consider the case of an exact resonance, with the influence of a weak detuning specified in Sec. V C. We assume further that none of the wave modes (and thus angular frequencies) coincide, with the special case of a 1:2 resonance also detailed in Sec. V C.

A. Multiple-scale analysis

For a triad evolving over the slow timescale $\tau = \epsilon t$, we posit the perturbation expansions

$$\eta(\boldsymbol{x}, t) \sim \eta_0(\boldsymbol{x}, t, \tau) + \epsilon\eta_1(\boldsymbol{x}, t, \tau) + O(\epsilon^2), \tag{12a}$$

$$u_l(\boldsymbol{x}, t) \sim u_{l,0}(\boldsymbol{x}, t, \tau) + \epsilon u_{l,1}(\boldsymbol{x}, t, \tau) + O(\epsilon^2) \quad \text{for} \quad l = 1, 2. \tag{12b}$$

We treat ϵ and t as independent variables, and hence treat t and $\tau = \epsilon t$ as independent timescales, with $\tau = O(1)$. By application of the chain rule, all time derivatives in the expanded Euler equations (4) are thus transformed according to the mapping $\partial_t \mapsto \partial_t + \epsilon\partial_\tau$. Finally, in a manner similar to Sec. IV, we denote the wave number, angular frequency, eigenfunction and Dirichlet-to-Neumann operators associated with each of the three wave modes by

$$K_j = k_{n_j}, \quad \Omega_j = \omega_{n_j}, \quad \Psi_j(\boldsymbol{x}) = \Phi_{n_j}(\boldsymbol{x}), \quad \text{and} \quad L_{l,j} = \hat{\mathscr{L}}_{l,n_j} \quad \text{for} \;\; j = 1, 2, 3 \;\; \text{and} \;\; l = 1, 2.$$

Upon substituting the perturbation expansions (12) into the asymptotic expansion of the Euler equations (4) and grouping together terms of size $O(1)$, we recover the linear equations

$$\frac{\partial \eta_0}{\partial t} + \mathscr{L}_1 u_{1,0} = 0, \quad \frac{\partial \eta_0}{\partial t} - \mathscr{L}_2 u_{2,0} = 0, \quad \frac{\partial}{\partial t}(u_{2,0} - \rho u_{1,0}) + (1 - \rho)\eta_0 = 0. \tag{13}$$

We posit that the leading-order solution is composed entirely of the three wave modes involved in the triad, namely

$$u_{l,0}(\boldsymbol{x},t,\tau) = \sum_{j=1}^{3}[A_{l,j}(\tau)\Psi_j(\boldsymbol{x})e^{-i\Omega_j t} + \text{c.c.}] \quad \text{for} \quad l = 1,2, \tag{14a}$$

$$\eta_0(\boldsymbol{x},t,\tau) = \sum_{j=1}^{3}[B_j(\tau)\Psi_j(\boldsymbol{x})e^{-i\Omega_j t} + \text{c.c.}], \tag{14b}$$

where $A_{1,j}(\tau)$, $A_{2,j}(\tau)$, and $B_j(\tau)$ denote the (as-yet-undetermined) complex amplitudes of each of the three wave modes ($j = 1, 2, 3$), and c.c. denotes the complex conjugate of the preceding term. Notably, $A_{1,j}(\tau)$ and $A_{2,j}(\tau)$ describe the slow evolution of the upper and lower velocity potentials, respectively, and $B_j(\tau)$ the free-surface displacement. The complex amplitudes are related by substituting into the leading-order equations (13), giving

$$A_{1,j}(\tau) = \frac{i\Omega_j}{L_{1,j}}B_j(\tau) \quad \text{and} \quad A_{2,j}(\tau) = \frac{-i\Omega_j}{L_{2,j}}B_j(\tau) \quad \text{for} \quad j = 1,2,3. \tag{15}$$

In order to determine evolution equations for each of the complex amplitudes, $A_{1,j}$, $A_{2,j}$, and B_j, we derive a solubility condition through consideration of higher-order terms in the perturbation expansion. Specifically, we substitute the perturbation expansion (12) and leading-order solution (14) into the asymptotic expansion of the Euler equations (4) and group together terms of size $O(\epsilon)$. As detailed in Appendix D, the first-order variables, η_1 and $u_{l,1}$, satisfy the inhomogeneous linear system

$$\frac{\partial \eta_1}{\partial t} + \mathscr{L}_1 u_{1,1} + \sum_{j=1}^{3}[F_{1,j}e^{-i\Omega_j t} + \text{c.c.}] = \text{n.r.t.}, \tag{16a}$$

$$\frac{\partial \eta_1}{\partial t} - \mathscr{L}_2 u_{2,1} + \sum_{j=1}^{3}[F_{2,j}e^{-i\Omega_j t} + \text{c.c.}] = \text{n.r.t.}, \tag{16b}$$

$$\rho\left(\frac{\partial u_{1,1}}{\partial t} + \eta_1 + \sum_{j=1}^{3}[G_{1,j}e^{-i\Omega_j t} + \text{c.c.}]\right) = \frac{\partial u_{2,1}}{\partial t} + \eta_1 + \sum_{j=1}^{3}[G_{2,j}e^{-i\Omega_j t} + \text{c.c.}] + \text{n.r.t.}, \tag{16c}$$

where n.r.t. denotes nonresonant terms, i.e., those of the form $p(\boldsymbol{x},\tau)e^{\pm i\varsigma t}$ with $\varsigma \notin \{\omega_0, \omega_1, \ldots\}$. The functions $F_{l,j}(\boldsymbol{x},\tau)$ and $G_{l,j}(\boldsymbol{x},\tau)$ (for $l = 1, 2$ and $j = 1, 2, 3$) are defined in Appendix D and consist of a combination of the wave amplitudes, $A_{l,j}(\tau)$ and $B_j(\tau)$, and the eigenfunctions, $\Psi_j(\boldsymbol{x})$.

To determine a solubility condition, we first project the first-order system (16) onto each of the three eigenfunctions, $\Psi_j(\boldsymbol{x})$. In a manner similar to Sec. III B, we remove the degeneracy in (16) by defining the independent variables $\hat{\xi}_{1,j} = (1-\rho)\langle\Psi_j, \eta_1\rangle$ and $\hat{\varphi}_{1,j} = \langle\Psi_j, u_{2,1} - \rho u_{1,1}\rangle$, which evolve according to (for $j = 1, 2, 3$)

$$\frac{\partial \hat{\xi}_{1,j}}{\partial t} - \Omega_j^2\hat{\varphi}_{1,j} + \Omega_j^2\left[\left\langle\Psi_j, \frac{\rho F_{1,j}}{L_{1,j}} + \frac{F_{2,j}}{L_{2,j}}\right\rangle e^{-i\Omega_j t} + \text{c.c.}\right] = \text{n.r.t.}, \tag{17a}$$

$$\frac{\partial \hat{\varphi}_{1,j}}{\partial t} + \hat{\xi}_{1,j} + [\langle\Psi_j, G_{2,j} - \rho G_{1,j}\rangle e^{-i\Omega_j t} + \text{c.c.}] = \text{n.r.t.} \tag{17b}$$

In (17), nonresonant terms (n.r.t.) correspond to those whose angular frequency differ from $\pm\Omega_j$. Recasting (17) as a matrix-vector system yields

$$\frac{\partial \boldsymbol{v}_j}{\partial t} + \boldsymbol{M}_j\boldsymbol{v}_j + [\boldsymbol{F}_j(\tau)e^{-i\Omega_j t} + \text{c.c.}] = \text{n.r.t.}, \quad \text{where} \quad \boldsymbol{v}_j = \begin{pmatrix}\hat{\xi}_{1,j}\\ \hat{\varphi}_{1,j}\end{pmatrix}, \quad \boldsymbol{M}_j = \begin{pmatrix}0 & -\Omega_j^2\\ 1 & 0\end{pmatrix},$$

and $\boldsymbol{M}_j$ has eigenvalues $\pm i\Omega_j$. By Fredholm's alternative theorem, a necessary condition for bounded solutions, $\boldsymbol{v}_j$, is that $\boldsymbol{F}_j(\tau)$ is orthogonal to a left-eigenvector of $\boldsymbol{M}_j$ with eigenvalue $i\Omega_j$. Specifically, the solubility condition is $\boldsymbol{w}_j^*\boldsymbol{F}_j = 0$, where $\boldsymbol{w}_j^* = (1, i\Omega_j)$ is a left-eigenvector satisfying $\boldsymbol{w}_j^*\boldsymbol{M}_j = i\Omega_j\boldsymbol{w}_j^*$. In terms of the functions $F_{l,j}(\boldsymbol{x},\tau)$ and $G_{l,j}(\boldsymbol{x},\tau)$, the solubility condition may be expressed as

$$i\Omega_j\left\langle \Psi_j, \frac{\rho F_{1,j}}{L_{1,j}} + \frac{F_{2,j}}{L_{2,j}}\right\rangle = \langle \Psi_j, G_{2,j} - \rho G_{1,j}\rangle \quad \text{for} \quad j = 1, 2, 3. \tag{18}$$

Each of these three conditions gives rise to an amplitude equation describing the evolution of the three wave modes involved in the triad.

By substituting the functions $F_{l,j}(\boldsymbol{x},\tau)$ and $G_{l,j}(\boldsymbol{x},\tau)$ into the solubility condition (18), we use the algebraic manipulations presented in Appendix D to determine that the free-surface displacement evolves according to the amplitude equations

$$2i\frac{\mathrm{d}B_1}{\mathrm{d}\tau} = \frac{\mathscr{C}\Gamma}{\Omega_2\Omega_3}B_2^*B_3^*, \quad 2i\frac{\mathrm{d}B_2}{\mathrm{d}\tau} = \frac{\mathscr{C}\Gamma}{\Omega_1\Omega_3}B_1^*B_3^*, \quad 2i\frac{\mathrm{d}B_3}{\mathrm{d}\tau} = \frac{\mathscr{C}\Gamma}{\Omega_1\Omega_2}B_1^*B_2^*, \tag{19}$$

where

$$\mathscr{C} = \frac{1}{S}\iint_{\mathcal{D}} \Psi_1\Psi_2\Psi_3\,\mathrm{d}A \tag{20}$$

is the correlation integral and S is the area of the cylinder cross section, $\mathcal{D}$ (see Sec. III). Furthermore, the triad coefficient, Γ, is defined as

$$\Gamma = \sum_{j=1}^{3} K_j^2\Lambda_j - \frac{1}{2}\big(K_1^2 + K_2^2 + K_3^2\big)\sum_{j=1}^{3}\Lambda_j - \frac{1}{2}\Omega_1\Omega_2\Omega_3\big[\Omega_1^2 + \Omega_2^2 + \Omega_3^2\big], \tag{21}$$

and

$$\Lambda_j = \frac{1}{\Omega_j(1-\rho)}\left[\frac{L_{2,j}}{L_{2,1}L_{2,2}L_{2,3}} - \frac{\rho L_{1,j}}{L_{1,1}L_{1,2}L_{1,3}}\right]\Omega_1^2\Omega_2^2\Omega_3^2 \quad \text{for } j = 1, 2, 3. \tag{22}$$

In addition to the temporal correlation condition $\Omega_1 + \Omega_2 + \Omega_3 = 0$, the triad equations (19) determine the two further necessary conditions specified in Sec. IV for three given wave modes to resonate: (i) the three modes must be correlated in space across the cylinder cross section, i.e., $\mathscr{C} \neq 0$ [23,25], and (ii) the triad coefficient must be nonzero, i.e., $\Gamma \neq 0$.

Although the triad equations (19) are of a form canonical to three-wave resonances (see Sec. 5 in Ref. [30]), two features are specific to our system. First, the correlation integral, $\mathscr{C}$, is a signature of the lateral confinement to a cylinder, with the condition $\mathscr{C} \neq 0$ being equivalent to $\boldsymbol{k}_1 + \boldsymbol{k}_2 + \boldsymbol{k}_3 = \boldsymbol{0}$ in unbounded domains with wave vectors $\boldsymbol{k}_j$. Second, the algebraic form of the triad coefficient, Γ, is unique to two-layer flows confined to a cylinder of finite height, and thus encodes the dependence of the triad evolution on the system parameters. However, the triad equations (19) also share commonalities with many other resonant three-wave systems arising in fluid mechanics. Specifically, the triad's energy, $\mathscr{E} = |B_1|^2 + |B_2|^2 + |B_3|^2$, is conserved [4,30], in accordance with the Hamiltonian form of the Euler equations, and the triad equations are integrable, with the solutions being periodic in time [32,33]. Of particular significance, however, is the relative timescale of the triad evolution, which we detail as follows.

B. Timescale of the triad evolution

As the product $\mathscr{C}\Gamma$ is common to all three triad equations (19), we deduce that $|\mathscr{C}\Gamma|^{-1}$ sets the relative timescale for the triad evolution. More efficient energy exchange between wave modes, corresponding to faster triad evolution, occurs for larger values of $|\mathscr{C}\Gamma|$, with energy exchange ceasing when $\mathscr{C} = 0$ or $\Gamma = 0$. The correlation integral, $\mathscr{C}$, depends only on the spatial form of the wave modes for a specified cross section of the cylinder and is thus independent of the density ratio

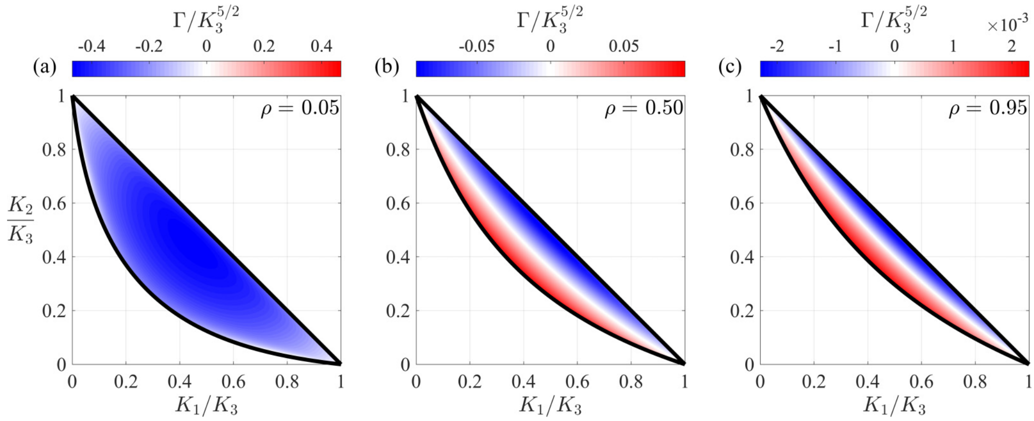

FIG. 4. The dependence of the triad evolution coefficient, Γ [defined in (21)], on the density ratio, $\rho = \rho_1/\rho_2$ and triad wave numbers, K_j. The depth of the upper layer is fixed at $h_1K_3 = 1$ (corresponding to the central column of Fig. 2) and the depth, h_2, of the lower layer satisfies $\Omega_1 + \Omega_2 + \Omega_3 = 0$, with $\Omega_1, \Omega_2 > 0$ and $\Omega_3 < 0$. (a) For $\rho \ll 1$, Γ approximates the triad coefficient, β, for one-layer flow [see (23)], which is strictly negative across the triad existence region [23]. [(b) and (c)] For larger ρ, Γ may be positive or negative, with triads existing only when $\Gamma \neq 0$. As ρ increases, the magnitude of Γ decreases according to the scaling $\Gamma = O((1-\rho)^{3/2})$ for $0 < 1 - \rho \ll 1$, thus dilating the triad evolution timescale.

and fluid depths. To gain insight into the influence of the system parameters on the efficiency of intratriad energy exchange, we thus focus instead on the value of Γ, which depends on the triad's wave numbers, K_j, density ratio, ρ, and the two fluid depths, h_1 and h_2. This dependence of Γ on the system parameters across the triad existence region is presented in Fig. 4, the pertinent features of which we detail as follows.

In the limit of strongly stratified flows, $\rho \to 0$, we note that $\Omega_j^2 \to L_j$ [see Eq. (8)], and so $\Lambda_j \to \Omega_j$ [see Eq. (22)]. Equation (21) and the condition $\Omega_1 + \Omega_2 + \Omega_3 = 0$ thus supply that $\Gamma \to \beta$ as $\rho \to 0$, where

$$\beta = \sum_{j=1}^{3} K_j^2\Omega_j - \frac{1}{2}\Omega_1\Omega_2\Omega_3\big[\Omega_1^2 + \Omega_2^2 + \Omega_3^2\big] \tag{23}$$

determines the triad evolution timescale for one-layer flows (see Eq. (4.13) in Ref. [23]). As $\beta < 0$ for all triads in the case $\Omega_1, \Omega_2 > 0$ and $\Omega_3 < 0$ [23], we deduce that the condition $\Gamma \neq 0$ is satisfied for all triads in the limit $\rho \to 0$. However, Γ vanishes near the left-hand boundary of the existence region for small values of ρ (corresponding to deep lower layers), as is evident by the white strips near the top left and bottom left of Fig. 4(a). The zero contour of Γ (white curve) moves further into the existence region as ρ is increased progressively [see Fig. 4(b)], dividing the existence region into portions with $\Gamma > 0$ (red) and $\Gamma < 0$ (blue). We note that the sign of Γ is immaterial to the triad dynamics and may be switched by mapping $\Omega_j \mapsto -\Omega_j$ for all j.

For weakly stratified flows, for which $0 < 1 - \rho \ll 1$, we note from Fig. 4(c) that Γ decreases in magnitude across the existence region, which we show to be consistent with the Boussinesq limit. Specifically, the timescale of the triad evolution diverges, corresponding to very slow energy exchange between the three wave modes. To quantify this time dilation, we expand the angular frequency of each wave mode, as defined in (8), in terms of the small parameter $\delta = 1 - \rho$, from which we deduce that (see Sec. 2 in Ref. [2])

$$\Omega_j^2 = \delta\widehat{\Omega}_j^2 + O(\delta^2), \quad \text{where } \widehat{\Omega}_j^2 = \frac{K_j}{\coth(K_jh_1) + \coth(K_jh_2)}. \tag{24}$$

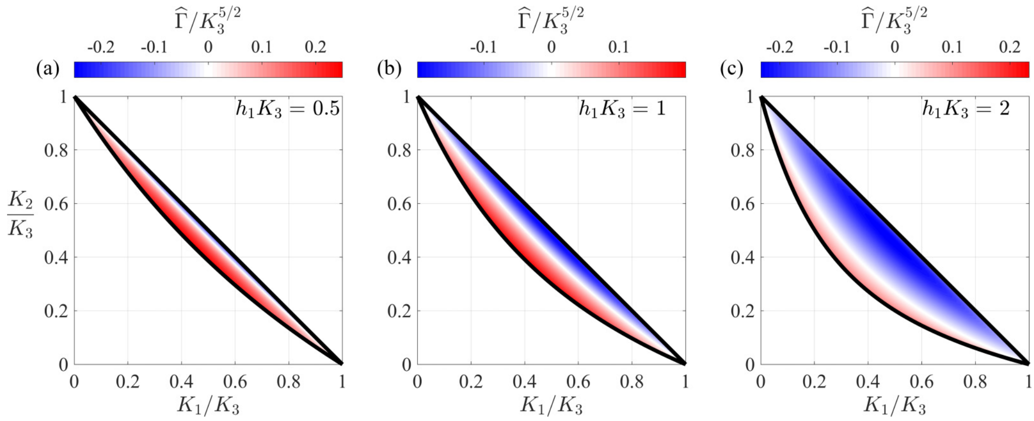

FIG. 5. The dependence of the Boussinesq triad evolution coefficient, $\widehat{\Gamma}$ [defined in (25)], on the depth of the upper layer across the triad existence region. The depth, h_2, of the lower layer satisfies $\widehat{\Omega}_1 + \widehat{\Omega}_2 + \widehat{\Omega}_3 = 0$, with $\widehat{\Omega}_1, \widehat{\Omega}_2 > 0$ and $\widehat{\Omega}_3 < 0$ [see (24)]. The depth of the upper layer assumes the values (a) $h_1K_3 = 0.5$, (b) $h_1K_3 = 1$, and (c) $h_1K_3 = 2$. Panel (b) is related to the triad coefficient presented in Fig. 4(c) according to the leading-order relationship $\Gamma = (1-\rho)^{3/2}\widehat{\Gamma}$ for $0 < 1-\rho \ll 1$.

Notably, truncating terms of $O(\delta^2)$ gives rise to the angular frequency deduced when applying the Boussinesq approximation (Sec. II B). Substituting this expansion for Ω_j^2 into (21) yields $\Gamma = \delta^{3/2}(\widehat{\Gamma} + O(\delta))$, where

$$\widehat{\Gamma} = \sum_{j=1}^{3} K_j^2\widehat{\Lambda}_j - \frac{1}{2}\left(K_1^2 + K_2^2 + K_3^2\right)\sum_{j=1}^{3}\widehat{\Lambda}_j \tag{25}$$

and

$$\widehat{\Lambda}_j = \frac{1}{\widehat{\Omega}_j}\left[\frac{L_{2,j}}{L_{2,1}L_{2,2}L_{2,3}} - \frac{L_{1,j}}{L_{1,1}L_{1,2}L_{1,3}}\right]\widehat{\Omega}_1^2\widehat{\Omega}_2^2\widehat{\Omega}_3^2.$$

To leading order in $\delta = 1-\rho$, the triad evolution equations (19) may thus be expressed as

$$2i\frac{\mathrm{d}B_1}{\mathrm{d}\tau} = \frac{\sqrt{1-\rho}\,\mathscr{C}\widehat{\Gamma}}{\widehat{\Omega}_2\widehat{\Omega}_3}B_2^*B_3^*, \quad 2i\frac{\mathrm{d}B_2}{\mathrm{d}\tau} = \frac{\sqrt{1-\rho}\,\mathscr{C}\widehat{\Gamma}}{\widehat{\Omega}_1\widehat{\Omega}_3}B_1^*B_3^*, \quad 2i\frac{\mathrm{d}B_3}{\mathrm{d}\tau} = \frac{\sqrt{1-\rho}\,\mathscr{C}\widehat{\Gamma}}{\widehat{\Omega}_1\widehat{\Omega}_2}B_1^*B_2^*,$$

from which we deduce that the triad evolution timescale is $O((1-\rho)^{-1/2})$ in the limit $\rho \to 1$, consistent with Boussinesq flows. The triad coefficient, Γ, thus retains a profile similar to that evident in Fig. 4(c) as $\rho \to 1$ (see Fig. 5), but its magnitude tends to zero across the existence region. The zero contour of $\widehat{\Gamma}$ (white curve) moves across the triad existence region (from right to left) as the depth of the upper layer, h_1K_3, is increased progressively.

C. Summary

For small-amplitude resonant triads confined to a cylinder in a two-layer system, the free surface evolves according to

$$\eta(\boldsymbol{x}, t) \sim \sum_{j=1}^{3}[B_j(\epsilon t)\Psi_j(\boldsymbol{x})e^{-i\Omega_j t} + \text{c.c.}] + O(\epsilon),$$

where $\Omega_1 + \Omega_2 + \Omega_3 = 0$ and the complex amplitudes, $B_j(\tau)$, satisfy the triad evolution equations (19). Furthermore, the wave modes must satisfy the correlation condition (9b) (or $\mathscr{C} \neq 0$)

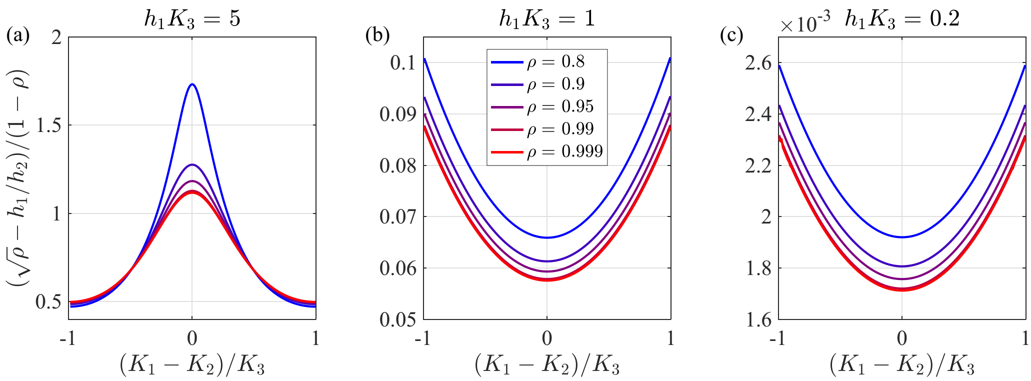

FIG. 6. Triad criticality for confined two-layer flows. Depth ratio, h_1/h_2, when $\Gamma = 0$ (white curve in Fig. 4) for (a) $h_1K_3 = 5$, (b) $h_1K_3 = 1$, and (c) $h_1K_3 = 0.2$. The critical depth ratio is compared to $\sqrt{\rho}$, the value at which criticality emerges for the two-layer KdV equation. The difference $\sqrt{\rho} - h_1/h_2$ is additionally scaled by $1-\rho$ to highlight the limiting behavior for weakly stratified flows, $0 < 1-\rho \ll 1$. (a) The deviation in the critical depth from a constant along the $\Gamma = 0$ contour is most pronounced for deeper fluids. (c) The difference between $\sqrt{\rho}$ and h_1/h_2 is smallest for long waves.

and the triad coefficient, Γ [as defined in (21)], must be nonzero. In accordance with the Boussinesq approximation, the timescale of the triad evolution for weakly stratified flows is $O((1-\rho)^{-1/2})$ and thus diverges as the density difference tends to zero. As with gravity waves in laterally unbounded domains [9], the correlation condition precludes the existence of resonant triads in rectangular cylinders (see Appendix A); nevertheless, resonant triads are found to be abundant in cylinders with nonrectangular cross sections, such as circles and annuli [23]. Specifically, the permissible triad combinations for two-layer flows are a subset of those emerging for one-layer flows, as follows from Corollary 1. It should also be noted that circular cylinders retain a continuous (azimuthal) symmetry that precludes some wave mode combinations, as the correlation condition (9b) requires that the azimuthal wave numbers, m_j, satisfies $m_1 + m_2 + m_3 = 0$ [22,23]. As the same restriction is not required for cylinders without azimuthal symmetry (e.g., for an elliptical cylinder), one would expect to sustain a far larger set of resonant triads in more complex geometries.

One key inference deduced from our analysis is that the triad coefficient, Γ, changes sign for particular combinations of wave numbers and fluid depths. This situation resembles the criticality emergent for the two-layer Korteweg–de Vries (KdV) equation, for which the coefficient of the quadratic term, $\eta\eta_x$, vanishes when $h_1/h_2 = \sqrt{\rho_1/\rho_2}$ [34], which simplifies to the condition $h_1 = h_2$ for Boussinesq flows [35]. This critical depth ratio is also apparent in our system for long waves or Boussinesq flows, yet substantial deviations and a notable dependence on the triad wave numbers emerge for deeper fluids with stronger stratification (see Fig. 6). In near-critical configurations, for which $\Gamma = O(\epsilon)$, the triad equations (19) cease to be valid; instead, one must consider terms of size $O(\epsilon^2)$ in the multiscale analysis. Finally, we note that the criticality for $\Gamma = O(\epsilon)$ differs from the small values of Γ identified for weakly stratified flows, for which $\Gamma = O((1-\rho)^{3/2})$): The latter scenario corresponds to a slow global evolution of the fluid system (including the oscillation of each wave mode), and so cubic terms need not be included in the asymptotic analysis in this case.

1. The influence of weak detuning

When there is a small discrepancy between the fluid depths and those required for a resonant triad, a weak detuning in the angular frequencies emerges. In the case when $\Omega_1 + \Omega_2 + \Omega_3 = \epsilon\sigma$ with $\sigma = O(1)$, the resulting amplitude equations are

$$2i\frac{\mathrm{d}B_1}{\mathrm{d}\tau} = \frac{\mathscr{C}\Gamma}{\Omega_2\Omega_3}B_2^*B_3^*e^{i\sigma\tau}, \quad 2i\frac{\mathrm{d}B_2}{\mathrm{d}\tau} = \frac{\mathscr{C}\Gamma}{\Omega_1\Omega_3}B_1^*B_3^*e^{i\sigma\tau}, \quad 2i\frac{\mathrm{d}B_3}{\mathrm{d}\tau} = \frac{\mathscr{C}\Gamma}{\Omega_1\Omega_2}B_1^*B_2^*e^{i\sigma\tau}. \tag{26}$$

The triad's wave energy, $\mathscr{E}$, oscillates weakly about its mean value, thus deviating slightly from the Hamiltonian structure of the Euler equations (see Sec. 5 in Ref. [30]). Nevertheless, the detuned triad equations are useful in practical applications, for which a small departure from a critical fluid depth is inevitable, and for characterizing intertriad coupling emerging for nearby critical depths [23]. We note, however, that when the frequency detuning from an exact triad becomes too large [i.e., when $\Omega_1 + \Omega_2 + \Omega_3 = O(1)$], the resonant triad ceases to exist and (26) no longer applies.

2. The case of a 1:2 resonance

A 1:2 resonance corresponds to a triad consisting of two copies of the same wave mode. The existence of 1:2 resonances may thus be established from the triad existence criteria stated in Sec. IV upon applying the mapping $(K_1, K_2, K_3) \mapsto (K_1, K_1, K_2)$ and may be visualized by considering the line $K_1 = K_2$ in Figs. 2–4. The angular frequencies, Ω_1 and Ω_2, of the two wave modes are thus related by $2\Omega_1 = \Omega_2$, where we consider $\Omega_1, \Omega_2 > 0$. Following a multiple-scale analysis similar to that presented in Sec. V A, we find that the free surface for standing waves in a 1:2 resonance evolves according to

$$\eta(\boldsymbol{x}, t) = \sum_{j=1}^{2} [B_j(\tau)\Psi_j(\boldsymbol{x})e^{-i\Omega_j t} + \text{c.c.}] + O(\epsilon),$$

where the complex amplitudes of the two wave modes satisfy

$$\frac{\mathrm{d}B_1}{\mathrm{d}\tau} = \frac{i\mathscr{C}\widetilde{\Gamma}}{4\Omega_1^2}B_1^*B_2 \quad \text{and} \quad \frac{\mathrm{d}B_2}{\mathrm{d}\tau} = \frac{i\mathscr{C}\widetilde{\Gamma}}{4\Omega_1^2}B_1^2. \tag{27}$$

The correlation integral in (27) is defined as $\mathscr{C} = (1/S)\iint_{\mathcal{D}} \Psi_1^2\Psi_2 \,\mathrm{d}A$ and the coefficient, $\widetilde{\Gamma}$, for a 1:2 resonance is derived from the triad coefficient, Γ [see (21)], via the mapping

$$(K_1, K_2, K_3, \Omega_1, \Omega_2, \Omega_3) \mapsto (K_1, K_1, K_2, \Omega_1, \Omega_1, -2\Omega_1).$$

The 1:2 resonance thus exhibits the same criticality phenomenon, i.e., $\widetilde{\Gamma} = 0$ for some parameter values, as triads.

Of particular interest is the case of a 1:2 resonance in a cylinder of circular or annular cross section, whose rotational symmetry [36,37] leads to a rich set of possible resonances. Based on the triad dynamics of single-layer flows (Table 1 in Ref. [23]), we anticipate that the following three resonant phenomena will emerge for a wide range of cylinder heights and density ratios: (i) the coupling of two standing waves [24], leading to a sloshing motion; (ii) the coupling of two copropagating waves, resulting in a steadily rotating wave profile [38,39]; and (iii) the coupling of an axisymmetric standing wave to counterpropagating, subharmonic and nonaxisymmetric wave modes [23], which together take a form analogous to an incident wave coupled to two traveling edge waves [40]. Enumerating all possible 1:2 resonances for different values of the density ratio and cylinder height is left as a matter for future consideration but may be deduced systematically by testing numerically all possible combinations of wave modes (see the Supplemental Material in Ref. [23]). Nevertheless, the variety of possible phenomena indicates the potential complexity of resonant dynamics emerging for two-layer gravity waves in closed basins.

VI. DISCUSSION

Density stratification and internal gravity waves play an important role in transferring energy in the world's oceans and large bodies of water. Our study demonstrates that lateral confinement of stratified fluids may amplify energy transfer within internal waves through the formation of resonant triads, representing a new mechanism for coupling internal seiche modes in geophysical basins

[21]. For the model problem of two-layer flow in a vertical cylinder with a rigid lid and base, our theoretical results determine criteria for the existence of critical depths at which three wave modes form a resonant triad. We also derived amplitude equations governing the long-time triad evolution, with which we quantified the relative efficiency of energy exchange for different triads and density ratios. The solutions to the triad equations are generally periodic, but quasiperiodic [41] and chaotic [23] solutions are possible when the system is resonantly forced [42]. The confined triads in our investigation are distinct from those emerging in the ocean, which require either a resonant interaction between internal and free-surface waves [4,8,16,17,19,32] or coupling between different vertical modes [3,43]. Our results thus lend new insight into the influence of lateral confinement on triad formation and have broader implications on the form of inverse energy cascades and weak turbulence of internal waves in confined basins [22,44,45].

The existence of resonant triads for two-layer flows shares some commonalities with the case of an air-liquid interface [22,23]. For both systems, resonant triads may form at certain critical depths, provided that the wave numbers comprising the triad lie within the triad existence region defined by Theorem 1. The wave modes must also be correlated in space, thus precluding the existence of resonant triads in rectangular cylinders. For two-layer flows, however, there exist curves in parameter space along which the triad interaction coefficient vanishes, representing a form of criticality evident in other two-layer systems [34,35] but absent for one-layer flows. The inclusion of a second fluid layer also suppresses the emergence of resonant triads in cylindrical geometries, with the existence region contained within that of one-layer flow (see Corollary 1) and vanishing when one of the fluid layers is very shallow. Nevertheless, resonant triads are still anticipated to be bountiful for two-layer flows in nonrectangular cylinders and geophysical basins.

The application of our theory to geophysical basins involves computing internal wave modes over an imposed variable bathymetry and incorporating viscous dissipation induced by liquid-boundary interactions [the latter of which would give rise to a damping term in the triad equations (19)]. Although the computation of wave modes in complex domains is a challenging task, reasonable approximations might be afforded using Defant's procedure [46] or by modeling the bathymetry by a series of steps of constant depth, representing stacked cylindrical basins. Our framework might also be generalized to include the effects of a finite-thickness pycnocline or the Coriolis force induced by planetary rotation. Nevertheless, the minimal two-layer system considered here contains the basic mechanisms necessary for resonantly coupling three internal wave modes of the lowest vertical order in a confined basin at a deep pycnocline. Our results for cylindrical basins are expected to be applicable to the formation of internal resonant triads in large and deep enclosed bodies of water with density stratification, including some deep lakes and seas.

Finally, the spatial correlation condition, $\mathscr{C} \neq 0$, points towards an emerging pattern governing the existence of resonant triads of sinusoidal wave modes. For rectangular cylinders, for which the wave modes are sinusoidal in both x and y, the correlation condition precludes the existence of resonant triads for both one- and two-layer flows [23]. For cylinders with rotational symmetry, for which the wave modes are sinusoidal in the azimuthal direction, the correlation condition restricts the permissible triad combinations to those whose angular wave numbers, m_j, satisfy $m_1 + m_2 = m_3$ [22,23]. For any cylindrical basin whose wave modes do not contain a sinusoidal component, however, numerical tests suggest that the correlation condition is nearly always satisfied, rendering triads abundant. A similar picture emerges for the existence of resonant triads in a continuously stratified fluid bounded above and below by rigid lids. For a constant density gradient, the wave modes are sinusoidal in the vertical direction and the triad interaction coefficients are nonzero only when an additional constraint on the vertical wave numbers is satisfied [47,48]. For all other stable stratification profiles, however, the vertical modes are nonsinusoidal and the interaction coefficients are nearly always nonzero, again rendering triads abundant [47]. Despite their ubiquity in physical systems, sinusoidal wave modes can thus restrict the formation of triads and so should be viewed as the exception, rather than the rule, when ascertaining which systems exhibit three-wave interactions.

ACKNOWLEDGMENTS

The authors thank Katarzyna N. Kowal for assistance with deriving (B2) and Zhan Wang for valuable discussions.

DATA AVAILABILITY

The data that support the findings of this article are openly available [49].

APPENDIX A: EXCLUSION OF RESONANT TRIADS FOR PLANE WAVES

We consider the linearized evolution of two-layer flows with means depths H_1 and H_2 and densities $\rho_1 < \rho_2$ in a stable stratification with gravitational acceleration g. The wave vector, $\boldsymbol{k}$, associated with plane-wave solutions of the form $e^{i(\boldsymbol{k}\cdot\boldsymbol{x}-\omega t)}$ is related to the angular frequency, ω, via the dispersion relation (see Sec. 231 in Ref. [29])

$$\omega(|\boldsymbol{k}|) = \sqrt{\frac{g(\rho_2-\rho_1)|\boldsymbol{k}|}{\rho_1\coth(|\boldsymbol{k}|H_1)+\rho_2\coth(|\boldsymbol{k}|H_2)}}. \tag{A1}$$

To prove that resonant triads of plane waves are impossible in laterally unbounded domains, we first prove that $\omega(k)$ is a positive, strictly increasing and strictly concave function of $k > 0$.

To prove that $\omega(k)$ is strictly increasing, we note that $\coth(x)$ is a strictly decreasing function for $x > 0$ and thus that $\coth(bx) > \coth(x)$ for $0 < b < 1$. We deduce that

$$\omega(bk) = \sqrt{\frac{g(\rho_2-\rho_1)bk}{\rho_1\coth(bkH_1)+\rho_2\coth(bkH_2)}} < \sqrt{\frac{g(\rho_2-\rho_1)k}{\rho_1\coth(kH_1)+\rho_2\coth(kH_2)}} = \omega(k), \tag{A2}$$

which shows that $\omega(k)$ is a strictly increasing function of $k > 0$. To prove that $\omega(k)$ is a strictly concave function for $k > 0$, we first recall that $\tanh(x)$ is a strictly concave function for $x > 0$ with $\tanh(0) = 0$, so that $\tanh(bx) > b\tanh(x)$ for $0 < b < 1$, or $\coth(bx) < b^{-1}\coth(x)$. The proof follows by noting that $\lim_{k\to 0}\omega(k) = 0$ and that

$$\omega(bk) = \sqrt{\frac{g(\rho_2-\rho_1)bk}{\rho_1\coth(bkH_1)+\rho_2\coth(bkH_2)}} > \sqrt{\frac{g(\rho_2-\rho_1)b^2k}{\rho_1\coth(kH_1)+\rho_2\coth(kH_2)}} = b\omega(k), \tag{A3}$$

which implies that $\omega(k)$ is a strictly concave function for all $k > 0$.

We now combine these two properties [Eqs. (A2) and (A3)] to show that resonant triads are impossible for plane waves with $\boldsymbol{k} \neq \boldsymbol{0}$. Specifically, a resonant triad would satisfy $\boldsymbol{k}_1 + \boldsymbol{k}_2 = \boldsymbol{k}_3$ and $\omega(|\boldsymbol{k}_1|) + \omega(|\boldsymbol{k}_2|) = \omega(|\boldsymbol{k}_3|)$. By the triangle inequality, we observe that $|\boldsymbol{k}_3| \leqslant |\boldsymbol{k}_1| + |\boldsymbol{k}_2|$. As $\omega(k)$ is a strictly increasing function for $k > 0$, we note that $\omega(|\boldsymbol{k}_3|) \leqslant \omega(|\boldsymbol{k}_1| + |\boldsymbol{k}_2|)$. Moreover, by the strict concavity of $\omega(k)$ for $k > 0$, we deduce that $\omega(|\boldsymbol{k}_1| + |\boldsymbol{k}_2|) < \omega(|\boldsymbol{k}_1|) + \omega(|\boldsymbol{k}_2|)$. By combining these two inequalities, we deduce that $\omega(|\boldsymbol{k}_3|) < \omega(|\boldsymbol{k}_1|) + \omega(|\boldsymbol{k}_2|)$, thereby violating the triad condition $\omega(|\boldsymbol{k}_1|) + \omega(|\boldsymbol{k}_2|) = \omega(|\boldsymbol{k}_3|)$. This proof is analogous to the case of free-surface gravity waves in single-layer flows [9,20].

APPENDIX B: PROOF OF THEOREM 1

Proof. To prove Theorem 1, we first show that there are no values of $h_2 \in (0, \infty)$ satisfying $\Omega_1 + \Omega_2 = \Omega_3$ when $K_1 + K_2 \geqslant K_3$, where we recall that

$$\Omega_j(h_2) = \sqrt{\frac{(1-\rho)K_j}{\rho\coth(K_jh_1)+\coth(K_jh_2)}}$$

and $K_j > 0$ for $j = 1, 2, 3$. We then prove that there exists a solution to $\Omega_1 + \Omega_2 = \Omega_3$ if and only if the inequalities (10) are satisfied and that the solution is unique.

In the case $K_1 + K_2 \geqslant K_3$, we first define

$$\omega(k) = \sqrt{\frac{(1-\rho)k}{\rho \coth(kh_1) + \coth(kh_2)}},$$

which is the dimensionless counterpart to the dispersion relation given in Eq. (A1). Notably, $\omega(K_j) = \Omega_j$ for $j = 1, 2, 3$. For fixed $h_2 > 0$, we recall from Appendix A that $\omega(k)$ is a positive, monotonically increasing, strictly concave function of $k > 0$. It thus follows that

$$\omega(K_3) \leqslant \omega(K_1 + K_2) < \omega(K_1) + \omega(K_2).$$

We conclude that $\Omega_3 < \Omega_1 + \Omega_2$ for any $h_2 > 0$, so there are no values of h_2 for which $\Omega_1 + \Omega_2 = \Omega_3$.

For the remainder of the proof, we consider the case

$$K_1 + K_2 < K_3, \tag{B1}$$

for which we will show that there exists a unique and finite value of $h_2 > 0$ satisfying $\Omega_1 + \Omega_2 = \Omega_3$ when the inequalities (10) are satisfied. Equivalently, we demonstrate that $F(h_2) = (\Omega_1(h_2) + \Omega_2(h_2))/\Omega_3(h_2) - 1$ has a unique positive root in this case, where we express

$$F(h_2) = \sqrt{\psi_1(h_2)} + \sqrt{\psi_2(h_2)} - 1$$

in terms of the positive functions ψ_1 and ψ_2 defined as

$$\psi_j(h_2) = \frac{K_j}{K_3}\left(\frac{\rho \coth(K_3 h_1) + \coth(K_3 h_2)}{\rho \coth(K_j h_1) + \coth(K_j h_2)}\right) \quad \text{for} \quad j = 1, 2.$$

Notably, the region $K_1 + K_2 < K_3$ is contained within the region $K_1 < K_3$ and $K_2 < K_3$. In fact, we prove that $F(h_2)$ is a strictly monotonically increasing function for all $h_2 > 0$ when $K_1 < K_3$ and $K_2 < K_3$, and is thus similarly increasing when $K_1 + K_2 < K_3$. To prove the monotonicity of $F(h_2)$, we compute (for $j = 1, 2$)

$$\frac{\mathrm{d}\psi_j}{\mathrm{d}h_2} = 2K_3\psi_j(h_2)\left(\frac{K_j/K_3}{f(K_j h_2)} - \frac{1}{f(K_3 h_2)}\right) > 0 \quad \text{for} \quad 0 < K_j < K_3,$$

where the inequality follows from the strict convexity of the positive function

$$f(x) = \sinh(2x) + 2\rho \sinh^2(x)\coth(\zeta x)$$

for all $x > 0$ [as shown in Eq. (B2) below], where $\zeta = h_1/h_2$ is a positive parameter and $\lim_{x\to 0} f(x) = 0$. Specifically, $f(bx) < bf(x)$ for all $x > 0$ and $0 < b < 1$, which implies that $b/f(bx) - 1/f(x) > 0$; the proof of the inequality follows by setting $x = K_3 h_2$ and $b = K_j/K_3$.

Given the strict monotonicity of $F(h_2)$ for $K_1 + K_2 < K_3$, we conclude that when a root of $F(h_2)$ exists, it is unique. In order to show the existence of a root of $F(h_2)$, we first note that

$$\lim_{h_2\to 0} F(h_2) = \frac{K_1 + K_2}{K_3} - 1 < 0,$$

where we have used that $\lim_{x\to 0}(x \coth(x)) = 1$ and implemented the inequality given in Eq. (B1). Moreover, we compute

$$\lim_{h_2\to\infty} F(h_2) = \sqrt{\frac{K_1}{K_3}}\sqrt{\frac{1 + \rho\coth(K_3 h_1)}{1 + \rho\coth(K_1 h_1)}} + \sqrt{\frac{K_2}{K_3}}\sqrt{\frac{1 + \rho\coth(K_3 h_1)}{1 + \rho\coth(K_2 h_1)}} - 1,$$

where we have used that $\lim_{x\to\infty}\coth(x) = 1$. As $F(h_2)$ is a continuous and strictly monotonically increasing function, the intermediate-value theorem determines that $F(h_2)$ has exactly one positive root if and only if the inequalities (10) are satisfied, corresponding to $\lim_{h_2\to\infty} F(h_2) > 0$ and $\lim_{h_2\to 0} F(h_2) < 0$.

To complete the proof, we show that $f(x)$ is a strictly convex function for all $x > 0$, where we decompose $f(x) = \sinh(2x) + 2\rho\sinh(x)\kappa(x)$, with $\kappa(x) = \sinh(x)\coth(\zeta x)$ and $\zeta > 0$. Notably, $\kappa(x)$ is a positive function for $x > 0$ and satisfies

$$\frac{\mathrm{d}\kappa}{\mathrm{d}x} = \frac{\zeta\cosh(x)}{\sinh^2(\zeta x)}\left[\frac{\sinh(2\zeta x)}{2\zeta} - \tanh(x)\right].$$

As $\tanh(x) < x < \sinh(2\zeta x)/(2\zeta)$ for all $x > 0$, we deduce that $\kappa(x)$ is a strictly monotonically increasing function. For all $x > 0$ and $0 < b < 1$, the strict convexity of $\sinh(x)$ (with $\sinh(0) = 0$) implies that $\sinh(bx) < b\sinh(x)$, and the strict monotonicity of $\kappa(x)$ implies that $\kappa(bx) < \kappa(x)$. We conclude, therefore, that

$$f(bx) = \sinh(2bx) + 2\rho\sinh(bx)\kappa(bx) < b\sinh(2x) + 2\rho b\sinh(x)\kappa(x) = bf(x). \tag{B2}$$

As $\lim_{x\to 0} f(x) = 0$, we deduce that $f(x)$ is a strictly convex function for all $x > 0$, thereby completing the proof. ■

APPENDIX C: EXISTENCE OF A TRIADS IN A CYLINDER OF FIXED HEIGHT

Resonant triads in a cylinder consisting of depths $h_2 = rh$ and $h_1 = (1-r)h$ must satisfy the condition $\Omega_1 + \Omega_2 = \Omega_3$ and thus arise when r is a root of the function $G(r) = (\Omega_1(r) + \Omega_2(r))/\Omega_3(r) - 1$. Based on numerical investigations, $G(r)$ is found to be a unimodal function that is maximized at $r = r_*$, where r_* depends on the system parameters and lies on the interval $0 < r_* < 1$. We note also that $G(0) = G(1) = K_1 + K_2 - K_3$. By combining these two properties with the first triad existence criterion, $K_1 + K_2 < K_3$, established in Theorem 1, we posit that resonant triads exist in a cylinder of finite depth when (i) $G(0) = G(1) < 0$ and (ii) $G(r_*) > 0$. When these criteria are satisfied, we compute the roots of $G(r)$ lying within the intervals $0 < r_{c,1} < r_*$ and $r_* < r_{c,2} < 1$. Finally, the left-most boundary of the triad existence region is defined as the curve along which $G(r_*) = 0$. Proving this triad existence criterion is left as a matter of future investigation, with the nonmonotonicity of $G(r)$ and the relatively complex dependence of Ω_j on r presenting the main challenges from an algebraic perspective.

APPENDIX D: DERIVATION OF THE TRIAD EQUATIONS

We proceed by substituting the perturbation expansion (12) into the asymptotic expansion of the Euler equations (4) and grouping together terms of size $O(\epsilon)$. The kinematic boundary conditions (4a) and (4b) give rise to the equations

$$\frac{\partial\eta_1}{\partial t} + \mathscr{L}_1 u_{1,1} + \left[\frac{\partial\eta_0}{\partial\tau} + \nabla\cdot(\eta_0\nabla u_{1,0})\right] = 0, \tag{D1a}$$

$$\frac{\partial\eta_1}{\partial t} - \mathscr{L}_2 u_{2,1} + \left[\frac{\partial\eta_0}{\partial\tau} + \nabla\cdot(\eta_0\nabla u_{2,0})\right] = 0, \tag{D1b}$$

and the dynamic boundary condition (4c) yields

$$\begin{aligned}\rho\left(\frac{\partial u_{1,1}}{\partial t} + \eta_1 + \left[\frac{\partial u_{1,0}}{\partial\tau} - \eta_0\frac{\partial}{\partial t}(\mathscr{L}_1 u_{1,0}) + \frac{1}{2}|\nabla u_{1,0}|^2 + \frac{1}{2}(\mathscr{L}_1 u_{1,0})^2\right]\right)\\ = \frac{\partial u_{2,1}}{\partial t} + \eta_1 + \left[\frac{\partial u_{2,0}}{\partial\tau} + \eta_0\frac{\partial}{\partial t}(\mathscr{L}_2 u_{2,0}) + \frac{1}{2}|\nabla u_{2,0}|^2 + \frac{1}{2}(\mathscr{L}_2 u_{2,0})^2\right].\end{aligned} \tag{D1c}$$

These three equations form a linear system for η_1, $u_{1,1}$, and $u_{2,1}$, where the inhomogeneous terms (denoted by square brackets) are composed of the leading-order solutions defined in Eq. (14). We thus substitute (14) into (D1) and group together terms that oscillate at angular frequencies Ω_1, Ω_2, and Ω_3, giving rise to Eq. (16). In (16), the functions $F_{1,1}(\boldsymbol{x},\tau)$ and $F_{2,1}(\boldsymbol{x},\tau)$ are defined as

$$F_{l,1} = \frac{\mathrm{d}B_1}{\mathrm{d}\tau}\Psi_1 - \Psi_2\Psi_3\left(K_3^2 B_2^* A_{l,3}^* + K_2^2 B_3^* A_{l,2}^*\right) + \nabla\Psi_2\cdot\nabla\Psi_3\left(B_2^* A_{l,3}^* + B_3^* A_{l,2}^*\right) \quad \text{for } l = 1, 2, \tag{D2a}$$

and the functions $G_{1,1}(\boldsymbol{x},\tau)$ and $G_{2,1}(\boldsymbol{x},\tau)$ are likewise defined as

$$\begin{aligned} G_{l,1} = {} & \frac{\mathrm{d}A_{l,1}}{\mathrm{d}\tau}\Psi_l + (-1)^l i\Psi_2\Psi_3\left(\Omega_3 L_{l,3} B_2^* A_{l,3}^* + \Omega_2 L_{l,2} B_3^* A_{l,2}^*\right) \\ & + \left(\nabla\Psi_2\cdot\nabla\Psi_3 + L_{l,2}L_{l,3}\Psi_2\Psi_3\right)A_{l,2}^* A_{l,3}^*. \end{aligned} \tag{D2b}$$

Finally, the functions $F_{l,j}(\boldsymbol{x},\tau)$ and $G_{l,j}(\boldsymbol{x},\tau)$ (for $j = 2, 3$) are defined by cyclic permutation of the indices (1, 2, 3).

In order to determine the amplitude equations, we proceed by substituting (D2) into the solubility condition (18), and then simplify by using that $\langle\Psi_1, \nabla\Psi_2\cdot\nabla\Psi_3\rangle = \frac{1}{2}\mathscr{C}(K_2^2 + K_3^2 - K_1^2)$ [25], where $\mathscr{C} = \langle\Psi_1, \Psi_2\Psi_3\rangle$ is the correlation integral (and likewise for cyclical permutation of the indices). Furthermore, we use (15) to eliminate $A_{1,j}$ and $A_{2,j}$ in terms of B_j. Finally, we use an equivalent form of the dispersion relation (8), namely

$$\frac{1}{L_{2,j}} + \frac{\rho}{L_{1,j}} = \frac{1-\rho}{\Omega_j^2},$$

to cancel common terms and simplify using $\Omega_1 + \Omega_2 + \Omega_3 = 0$. After some lengthy algebra, the solubility condition (18) gives rise to the three evolution equations:

$$\frac{\mathrm{d}B_1}{\mathrm{d}\tau} = \frac{i\Omega_1\mathscr{C}\gamma}{2(1-\rho)}B_2^*B_3^*, \quad \frac{\mathrm{d}B_2}{\mathrm{d}\tau} = \frac{i\Omega_2\mathscr{C}\gamma}{2(1-\rho)}B_1^*B_3^*, \quad \frac{\mathrm{d}B_3}{\mathrm{d}\tau} = \frac{i\Omega_3\mathscr{C}\gamma}{2(1-\rho)}B_1^*B_2^*, \tag{D3}$$

where

$$\begin{aligned} \gamma = {} & \left(K_2^2 + K_3^2 - K_1^2\right)\frac{\Omega_2\Omega_3}{2}\left[\frac{1}{L_{2,2}L_{2,3}} - \frac{\rho}{L_{1,2}L_{1,3}}\right] + \left(K_3^2 + K_1^2 - K_2^2\right)\frac{\Omega_3\Omega_1}{2}\left[\frac{1}{L_{2,3}L_{2,1}} - \frac{\rho}{L_{1,3}L_{1,1}}\right] \\ & + \left(K_1^2 + K_2^2 - K_3^2\right)\frac{\Omega_1\Omega_2}{2}\left[\frac{1}{L_{2,1}L_{2,2}} - \frac{\rho}{L_{1,1}L_{1,2}}\right] + \frac{(1-\rho)}{2}\left[\Omega_1^2 + \Omega_2^2 + \Omega_3^2\right]. \end{aligned} \tag{D4}$$

By defining

$$\lambda_j = \frac{\Omega_1\Omega_2\Omega_3}{\Omega_j}\left[\frac{L_{2,j}}{L_{2,1}L_{2,2}L_{2,3}} - \frac{\rho L_{1,j}}{L_{1,1}L_{1,2}L_{1,3}}\right], \tag{D5}$$

and rewriting $K_2^2 + K_3^2 - K_1^2 = (K_1^2 + K_2^2 + K_3^2) - 2K_1^2$, etc., we recast γ in the more compact form

$$\gamma = \frac{1}{2}\left(K_1^2 + K_2^2 + K_3^2\right)\sum_{j=1}^{3}\lambda_j - \sum_{j=1}^{3}\lambda_j K_j^2 + \frac{(1-\rho)}{2}\left(\Omega_1^2 + \Omega_2^2 + \Omega_3^2\right). \tag{D6}$$

Finally, we obtain the triad equations presented in Eqs. (19)–(22) by defining

$$\Gamma = \frac{-\Omega_1\Omega_2\Omega_3}{1-\rho}\gamma \quad \text{and} \quad \Lambda_j = \frac{\Omega_1\Omega_2\Omega_3}{1-\rho}\lambda_j \quad \text{for} \quad j = 1, 2, 3,$$

and substituting into Eqs. (D4)–(D6).

[1] W. M. Munk, Abyssal recipes, Deep-Sea Res. **13**, 707 (1966).
[2] B. R. Sutherland, *Internal Gravity Waves* (Cambridge University Press, Cambridge, UK, 2010).
[3] S. A. Thorpe, On wave interactions in a stratified fluid, J. Fluid Mech. **24**, 737 (1966).
[4] F. K. Ball, Energy transfer between external and internal gravity waves, J. Fluid Mech. **19**, 465 (1964).
[5] P. G. Baines, Waves in stratified fluids, in *Topographic Effects in Stratified Flows*, Cambridge Monographs on Mechanics (Cambridge University Press, Cambridge, UK, 2022), pp. 196–242.
[6] M. Carr, P. A. Davies, and R. P. Hoebers, Experiments on the structure and stability of mode-2 internal solitary-like waves propagating on an offset pycnocline, Phys. Fluids **27**, 046602 (2015).
[7] R. Barros, W. Choi, and P. A. Milewski, Strongly nonlinear effects on internal solitary waves in three-layer flows, J. Fluid Mech. **883**, A16 (2020).
[8] H. Segur, Resonant interactions of surface and internal gravity waves, Phys. Fluids **23**, 2556 (1980).
[9] O. M. Phillips, On the dynamics of unsteady gravity waves of finite amplitude. Part 1. The elementary interactions, J. Fluid Mech. **9**, 193 (1960).
[10] D. J. Benney, Non-linear gravity wave interactions, J. Fluid Mech. **14**, 577 (1962).
[11] M. S. Longuet-Higgins, Resonant interactions between two trains of gravity waves, J. Fluid Mech. **12**, 321 (1962).
[12] R. E. Davis and A. Acrivos, The stability of oscillatory internal waves, J. Fluid Mech. **30**, 723 (1967).
[13] A. McEwan, Degeneration of resonantly-excited standing internal gravity waves, J. Fluid Mech. **50**, 431 (1971).
[14] B. R. Sutherland and R. Jefferson, Triad resonant instability of horizontally periodic internal modes, Phys. Rev. Fluids **5**, 034801 (2020).
[15] Q. Pan, N. N. Peng, H. N. Chan, and K. W. Chow, Coupled triads in the dynamics of internal waves: Case study using a linearly stratified fluid, Phys. Rev. Fluids **6**, 024802 (2021).
[16] T. M. Joyce, Nonlinear interactions among standing surface and internal gravity waves, J. Fluid Mech. **63**, 801 (1974).
[17] T. M. A. Taklo and W. Choi, Group resonant interactions between surface and internal gravity waves in a two-layer system, J. Fluid Mech. **892**, A14 (2020).
[18] M.-R. Alam, A new triad resonance between co-propagating surface and interfacial waves, J. Fluid Mech. **691**, 267 (2012).
[19] W. Choi, M. Chabane, and T. M. A. Taklo, Two-dimensional resonant triad interactions in a two-layer system, J. Fluid Mech. **907**, A5 (2021).
[20] K. Hasselmann, On the non-linear energy transfer in a gravity-wave spectrum. Part 1. General theory, J. Fluid Mech. **12**, 481 (1962).
[21] U. Lemmin, C. H. Mortimer, and E. Bäuerle, Internal seiche dynamics in Lake Geneva, Limnol. Oceanogr. **50**, 207 (2005).
[22] G. Michel, Three-wave interactions among surface gravity waves in a cylindrical container, Phys. Rev. Fluids **4**, 012801(R) (2019).
[23] M. Durey and P. A. Milewski, Resonant triad interactions of gravity waves in cylindrical basins, J. Fluid Mech. **966**, A25 (2023).
[24] L. R. Mack, Periodic, finite-amplitude, axisymmetric gravity waves, J. Geophys. Res. **67**, 829 (1962).
[25] J. W. Miles, Nonlinear surface waves in closed basins, J. Fluid Mech. **75**, 419 (1976).
[26] J. W. Miles, Internally resonant surface waves in a circular cylinder, J. Fluid Mech. **149**, 1 (1984).
[27] J. W. Miles and D. M. Henderson, Parametrically forced surface waves, Annu. Rev. Fluid Mech. **22**, 143 (1990).
[28] R. K. Zeytounian, Joseph Boussinesq and his approximation: A contemporary view, C. R. Mec. **331**, 575 (2003).
[29] H. Lamb, *Hydrodynamics*, 6th ed. (Dover, New York, 1932).
[30] A. D. D. Craik, *Wave Interactions and Fluid Flows*, Cambridge Monographs on Mechanics (Cambridge University Press, Cambridge, UK, 1986).
[31] J. K. Kevorkian and J. D. Cole, *Multiple Scale and Singular Perturbation Methods*, Applied Mathematical Sciences Vol. 114 (Springer, New York, 1996).

[32] W. F. Simmons, A variational method for weak resonant wave interactions, Proc. R. Soc. Lond. A **309**, 551 (1969).

[33] F. Bretherton, Resonant interactions between waves. The case of discrete oscillations, J. Fluid Mech. **20**, 457 (1964).

[34] W. Choi and R. Camassa, Fully nonlinear internal waves in a two-fluid system, J. Fluid Mech. **396**, 1 (1999).

[35] F. Dias and J.-M. Vanden-Broeck, Steady two-layer flows over an obstacle, Philos. Trans. R. Soc. A. **360**, 2137 (2002).

[36] T. J. Bridges and F. Dias, An analysis of two-dimensional water waves based on O(2) symmetry, Nonlin. Anal. Theory Methods Appl. **14**, 733 (1990).

[37] P. Chossat and F. Dias, The 1:2 resonance with O(2) symmetry and its applications in hydrodynamics, J. Nonlinear Sci. **5**, 105 (1995).

[38] P. J. Bryant, Nonlinear progressive free waves in a circular basin, J. Fluid Mech. **205**, 453 (1989).

[39] X. Yang, F. Dias, Z. Liu, and S. Liao, Finite-amplitude steady-state resonant waves in a circular basin, J. Fluid Mech. **915**, A136 (2021).

[40] R. T. Guza and R. E. Davis, Excitation of edge waves by waves incident on a beach, J. Geophys. Res. **79**, 1285 (1974).

[41] J. Harris, M. D. Bustamante, and C. Connaughton, Externally forced triads of resonantly interacting waves: Boundedness and integrability properties, Commun. Nonlin. Sci. Numer. Simulat. **17**, 4988 (2012).

[42] D. Mackey and E. A. Cox, Dynamics of a two-layer fluid sloshing problem, IMA J. Appl. Math. **68**, 665 (2003).

[43] C. F. M. Raupp, P. L. Silva Dias, E. G. Tabak, and P. A. Milewski, Resonant wave interactions in the equatorial waveguide, J. Atmos. Sci. **65**, 3398 (2008).

[44] Z. Taebel, M. L. McAllister, A. Scotti, M. Onorato, and T. S. van den Bremer, Laboratory study of wave turbulence under isotropic forcing, Phys. Rev. Fluids **9**, 094803 (2024).

[45] S. M. D. Gregory, S. Schiattarella, V. S. Barroso, D. I. Kaiser, A. Avgoustidis, and S. Weinfurtner, Tracking the nonlinear formation of an interfacial wave spectral cascade from one to few to many, arXiv:2410.08842 [gr-qc].

[46] U. Lemmin and C. H. Mortimer, Tests of an extension to internal seiches of Defant's procedure for determination of surface seiche characteristics in real lakes, Limnol. Oceanogr. **31**, 1207 (1986).

[47] D. Varma and M. Mathur, Internal wave resonant triads in finite-depth non-uniform stratifications, J. Fluid Mech. **824**, 286 (2017).

[48] T. R. Akylas and C. Kakoutas, Stability of internal gravity wave modes: From triad resonance to broadband instability, J. Fluid Mech. **961**, A22 (2023).

[49] See Supplemental Material at http://link.aps.org/supplemental/10.1103/m657-9blf for MATLAB code used to generate Figs. 2–6.